Journal of Statistical Physics, Vol. 68, Nos. 5/6, 1992

Diffusion, Effusion, and Chaotic Scattering: An Exactly Solvable Liouvillian Dynamics

Pierre Gaspard[1]

Received November 21, 1991; final March 10, 1992

We study diffusion and chaotic scattering in a chain of baker maps coupled together which forms an area-preserving mapping of an infinitely extended strip onto itself. This exactly solvable mapping sustains chaotic behaviors and diffusion processes. The relationship between the diffusion coefficient, the Lyapunov exponent, and the entropy per unit time is derived. The long-lived classical resonances of the Liouville evolution operator are proved to converge toward the eigenvalues of the phenomenological diffusion equation. In this sense, there is a quasi-isomorphism between the resonance spectrum of the Liouville evolution and the eigenvalue spectrum of the phenomenological diffusion equation. Furthermore, we show that a fractal repeller is associated to each nonequilibrium state in the isolated and finite multibaker chain. The nonequilibrium states are all unstable with respect to the equilibrium, validating a weak form of the second principle of thermodynamics for the present dynamical system. Consequences of nonequilibrium fractals on classical measurements are discussed. We then describe the open multibaker chain as a scattering system. Fractal properties of chaotic scattering are here shown to be related to diffusion in the chain.

KEY WORDS: Nonequilibrium fractal repeller; zeta function; Ruelle resonance; dynamical chaos; irreversibility.

1. INTRODUCTION

The recent developments in the field of chaotic dynamics are focusing more and more on large systems of interest in statistical mechanics[1-9],[2] and are

[1] Faculté des Sciences, Université Libre de Bruxelles, Campus Plaine, Code Postal 231, B-1050 Brussels, Belgium.

[2] In refs. 4 and 5, the authors assume a Nosé–Hoover dissipative coupling between the fluid and the reservoirs. As a consequence, there appears a chaotic attractor in phase space. We believe that this dissipative assumption is artificial and unnecessary. On the other hand, the fractal repellers we consider here arise in Hamiltonian systems without any dissipative assumption and are intrinsic to the system. In Section 6 we show that the coupling to reservoirs can be considered as Poisson statistical processes over the dynamical system, a definition which preserves the Hamiltonian character of the time evolution.

0022-4715/92/0900-0673$06.50/0

gradually suggesting that dynamical chaos is the new paradigm for understanding irreversible processes. Interacting classical gases, liquids, or solids are typically nonlinear dynamical systems ruled by a Hamiltonian like

$$H = \sum_{i=1}^{N} \frac{p_i^2}{2m} + \sum_{1 \leqslant i < j \leqslant N} V(r_{ij}) \tag{1.1}$$

and confined in a container. These systems present the property of sensitivity to initial conditions already at the microscopic level of the motion of atoms and molecules in the gas. This sensitivity to initial conditions is characterized by the Lyapunov exponents, which are the rates of exponential separation between nearby trajectories.[10 14] In many-body systems, there are as many positive Lyapunov exponents as independent stretching directions. Because the Hamiltonian systems are time-reversal symmetric and have a symplectic structure, a direction of contraction with a negative Lyapunov exponent corresponds to each stretching direction.

In closed systems, the exponential separation of nearby trajectories cannot continue forever in a global way, so that folding of phase space volumes rapidly follows the first stage of stretching. This folding mechanism and the reinjection into the initial phase space volume generate dynamical randomness which is itself characterized by the Kolmogorov–Sinai (KS) entropy per unit time. In closed hyperbolic dynamical systems, the KS entropy is equal to the sum of the positive Lyapunov exponents according to Pesin's formula.[14,15]

The entropy per unit time appears to be proportional to the number of particles in many-body classical systems. This result suggests the introduction of the entropy per unit time and volume.[16] Recent work has been devoted to the estimation of this quantity, which is of order of 10^{30} digits/sec cm^3 in typical interacting gases.[4,6,7] This microscopic chaos must be distinguished from the recently studied macroscopic chaos arising from the nonlinear coupling between the hydrodynamic modes of far-from-equilibrium physicochemical systems. The known examples of chaos at the macroscopic level present KS entropies of the order of 0.01–100 digits/sec.[17] In celestial mechanics, chaotic systems have a much lower power of dynamical randomness: for instance, Hyperion has a KS entropy of the order of 5×10^{-8} digits/sec.[18] On the other hand, microscopic chaos takes place on a much shorter time scale, of the order of the mean intercollisional time between the atoms or molecules.[7]

We arrive at the important result that interacting many-body systems without a hierarchy of constants of motion may be characterized in many cases by a positive entropy per unit time and volume, in contrast to the ideal gases and the harmonic solid, which have a vanishing entropy per

unit time and volume.[16,19],[3] This feature is reminiscent of the fact that the ideal gases cannot sustain transport processes. In a different but related context, work on transport processes in few-degree-of-freedom Hamiltonian or conservative systems by Kadanoff, MacKay, Meiss, and others is also giving evidence that transport properties have their origin in the chaotic dynamics and the related Poincaré–Birkhoff homoclinic tangles.[20]

Our purpose in the present paper is to demonstrate the existence of relationships between microscopic chaos and the transport properties of statistical mechanics, as suggested by the previous discussion. We shall here focus on diffusion in real space. The vehicle we use for this program is a simple and exactly solvable deterministic dynamical system of large spatial extension that we construct here for the first time. Our model is formed by a chain of coupled baker transformations.

The baker transformation is a well-known example of a Bernoulli map which has been extensively studied in the last decades as a simple deterministic dynamical system showing the ergodic property of mixing, Kolmogorov, and Bernoulli[11]:

$$\Phi_b(x, y) = \begin{cases} (2x, y/2) & 0 \leqslant x < 1/2, \quad 0 \leqslant y < 1 \\ (2x-1, y/2+1/2) & 1/2 \leqslant x < 1, \quad 0 \leqslant y < 1 \end{cases} \tag{1.2}$$

This famous mapping was described in the book by Hopf on ergodic theory[21] and later in the book by Arnold and Avez.[11] The baker transformation is an area-preserving map on the unit square with a chaotic dynamics where many dynamical properties can be illustrated, such as construction of the symbolic dynamics, proof of the central limit theorem for a large class of functions showing that the dynamical fluctuations are Gaussian, and calculation of several correlation functions and of the correlation decay rates. The success of this model contributed to the invention of related models, such as piecewise-linear 2D area-contracting maps with chaotic attractors[22] or area-preserving 2D maps isomorphic to Bernoulli processes with more than two symbols, or to Markov chains. A related class of simple maps is the famous Smale horseshoe and its variants.[23]

Similar mappings have been invented with the purpose of modeling some physicochemical processes such as chemical reactions and, in

[3] The ideal gas is known to have an infinite KS entropy per unit time. This infinity has been shown[19] to arise from the logarithmic divergence of the ε-entropy per unit time of the ideal gas, where ε is the volume of an infinitesimal cell in phase space. However, the ε-entropy per unit time is proportional to the area of a surface crossed by particles. As a consequence, the ε-entropy per unit time divided by the volume, i.e., the ε-entropy per unit time and unit volume, vanishes for all ε in the limit of large volume.

particular, isomerization. In this context, Elskens and Kapral proposed in 1985 a model of isomerization where three baker maps are coupled together.[24] The phase space is composed of two joined unit squares where two independent bakers act during a first step. In a second step, a third baker acts on the unit square composed of two contiguous halves of the two original unit squares. A rate process is thus induced between the two unit squares representing two states of a molecule.

In the present paper, we describe a generalization of this model by coupling in a similar way a large number of baker transformations acting on a chain of squares. When the chain of squares extends to infinity, a diffusion process is induced along the chain by the chaotic dynamics of stretching and folding characteristic of the baker transformations. We shall call it the multibaker chain or multibaker mapping. Because the deterministic dynamics is piecewise-linear, its theoretical analysis is simple. As another tractable model of diffusion we mention the finite-horizon Lorentz gas studied by Bunimovich and Sinai[25] and Machta and Zwanzig.[26]

As pieces of material can be put into different experimental conditions by changing the boundary conditions, we can consider the multibaker chain as (1) infinite, (2) finite and isolated, or (3) finite and open, with or without a continuous flow of particles.

In the isolated chain, we study relaxation dynamics to equilibrium, calculating the spectrum of the decay rates. We use the new methods developed in the theory of dynamical systems and based on the periodic orbits of the system.[8,27–34] To introduce these new methods, let us recall the context of their development. In the well-known Koopman approach to classical dynamics[35] the linear evolution operator

$$(U^t f)(X) = f(\Phi^t X) \tag{1.3}$$

is associated to Hamiltonian flows like (1.1). $\Phi^t X$ denotes the trajectory of (1.1) from the initial conditions $X = (\mathbf{q}, \mathbf{p})$. Here $f(X)$ is a function defined in phase space. When the function $f(X)$ belongs to the Hilbert space $\mathscr{L}^2(\mu)$ constructed with the inner product based on the Liouville invariant measure μ, the evolution operator U^t turns out to be a unitary operator. For continuous-time flows, U^t can be written like

$$U^t = \exp itL \tag{1.4}$$

in terms of the Lie group generator L, which is the Hermitian operator called the Liouvillian[36]

$$L = i\{H, \cdot\} = i\sum_k \left(\frac{\partial H}{\partial q_k}\frac{\partial}{\partial p_k} - \frac{\partial H}{\partial p_k}\frac{\partial}{\partial q_k} \right) \tag{1.5}$$

The eigenvalues of this operator can only be real, forming a spectrum which is pointlike, singular, or continuous. This result is at the origin of a number of paradoxes and difficulties in our understanding of relaxation toward equilibrium. In the new approach by Mayer, Roepstorff, Ruelle, and others, the evolution operator (1.3) or its adjoint is extended and allowed to act on Schwartz distributions.[27–31],[4] In this generalization, the evolution operator acquires a spectrum formed by complex eigenvalues or resonances corresponding to eigendistributions. The resonances can be obtained as poles of Ruelle's zeta functions defined from the periodic orbits of the system. The imaginary parts of the resonances give the decay rates of the relaxation to equilibrium. Ruelle's zeta functions[28] and their poles, known as Ruelle's resonances,[31–34] can here be explicitly calculated and shown to give the decay rates of a diffusive dynamics for the isolated multibaker chain.

On the other hand, the dynamics in the open chain appears as a typical chaotic scattering process. The scattering map is shown to have singularities on a fractal set of ingoing trajectories. Chaotic scattering has been much studied recently in systems with a few scatterers and, in particular, in the three-disk scatterer.[8,30,37,38] With the multibaker chain as well as with the open Lorentz gas described in ref. 9 we extend the study of chaotic scattering to systems of statistical mechanics, where we find deep and fruitful connections with transport properties, as shown in the following sections. In the open chain, Ruelle's resonances obtained from the zeta function appear as the classical analogue of the quantum scattering resonances.[8]

The paper is composed of six parts. In Section 2 we describe the spectral theory of the classical evolution operator enriched with the concepts of Ruelle's zeta function and of classical scattering resonances. We show in this section how the relaxation and decay rates of a dynamical system can be calculated as resonances.

In Section 3 we define the multibaker map of infinite extension where diffusion occurs. The diffusion coefficient is there calculated and related to the velocity autocorrelation function.

In Section 4 we construct the closed and finite chain of baker transformations. Nonequilibrium states are defined by absorbing boundaries. On one hand, we show how this first-passage problem generates a fractal set

[4] We give an example of an eigendistribution for the simple area-preserving mapping, which is $\Phi(x, y) = (\Lambda x, \Lambda^{-1} y)$. The invariant set is a periodic orbit of saddle type at the origin. The escape rates of this repeller are $\gamma_k = (k+1) \ln \Lambda$ of multiplicity $k+1$ ($k \in N$). The Schwartz distributions corresponding to these complex eigenvalues are $\psi_{k,l}(x, y) = y^{k-l} \delta^{(l)}(x)$ ($l = 0, \ldots, k$), where $\delta^{(l)}$ is the lth derivative of the Dirac distribution. These eigendistributions satisfy $U\psi_{k,l} = [\exp(-\gamma_k)]\psi_{k,l}$.

of trapped trajectories in a one-particle system, and, on the other hand, we treat the problem of density fluctuations between two parts of the finite chain following a suggestion by Eckmann and Rand. We prove that each nonequilibrium state is dynamically unstable since it is a fractal of saddle type with a positive escape rate and a fractional Hausdorff dimension. In contrast, the equilibrium state is stable with a zero escape rate because it fills the whole phase and has a Hausdorff dimension equal to two. In this way, we establish a relation with the second principle of thermodynamics.

In Section 5 we consider the open and finite chain of baker transformations and we calculate exactly the spectrum of the scattering resonances for its evolution operator. We show how large-scale diffusion is related to chaotic scattering and the presence of a fractal repeller. In particular, we derive the relation between the diffusion coefficient, the Lyapunov exponent, and the entropy per unit time, as well as with the information dimension of the repeller.

In Section 6 a concentration gradient is built in the open and finite multibaker chain to describe a nonequilibrium continuous flow of particles. We define here the nonequilibrium process as a Poisson suspension over the dynamical system. Fick's law is shown to hold on the chain.

Conclusions are drawn in Section 7, where we discuss the extension of the methods developed here to other more realistic models such as the Lorentz gas, the hard-sphere gas, or the Lennard-Jones gas.

2. EVOLUTION OPERATOR AND ITS RESONANCES

The aim of this section is to recall some results about the spectral properties of the classical evolution operator as extension of the Koopman operator,[35] which acts on functions defined over phase space. In particular, we shall expose the new methods based on the concept of classical scattering resonances.

2.1. Hyperbolic Systems

In this paper, we shall study mappings for which several assumptions are made. In particular, we suppose that the system is hyperbolic, so that every trajectory is unstable of saddle type.[14,23,27] Recent work on classical systems has shown that a central role is played by the these hyperbolic zones to induce transport in phase space.[20]

The dynamical system is supposed to be a two-dimensional mapping

$$X_t = \Phi^t X_0, \qquad X = (x, y) \tag{2.1}$$

where the time t is discrete ($t \in \mathbf{Z}$). The mapping acts in a phase space $\mathscr{M}$ which may be bounded or unbounded. If the phase space is unbounded and extends to infinity, as well as in nonequilibrium problems in large, bounded phase space, we shall consider the restricted system formed by the trajectories which are indefinitely trapped in a bounded domain $\mathscr{V}$ of $\mathscr{M}$. The mapping Φ is assumed to be area-preserving in the sense that the determinant of its Jacobian matrix is unity:

$$\text{for} \quad J = \frac{\partial \Phi}{\partial X}, \qquad \det J(X) = 1, \qquad \forall X \in \mathscr{M} \tag{2.2}$$

In the domain $\mathscr{V}$ (or in the whole space $\mathscr{M}$ if it is bounded), the mapping is assumed to be hyperbolic, i.e., any trajectory $\Phi^t X$ is unstable of saddle type. Stable and unstable manifolds are associated to each trajectory. In the following sections, the mapping will even be uniformly hyperbolic, i.e., the stable and unstable manifolds have always the same directions and the stretching and contracting factors are constant everywhere, for instance, the absolute values Λ and Λ^{-1}, respectively. Each periodic or nonperiodic trajectory possesses thus a positive and a negative Lyapunov exponents of equal absolute value because of the area-preserving property

$$\lambda = \lambda_u = -\lambda_s = \frac{1}{\tau} \ln \Lambda \tag{2.3}$$

where τ is the time unit taken to perform one iteration Φ. The mapping Φ is also time-reversal symmetric in the sense that there exists a transformation T such that

$$\Phi^{-1} = \mathrm{T} \circ \Phi \circ \mathrm{T} \tag{2.4}$$

which is an involution, $\mathrm{T}^2 = 1$.

2.2. Liouville Dynamics and Its Complex Resonances

The mapping induces a time evolution for measurable function $\mathscr{E} = \{f(X)\}$ defined on the phase space $\mathscr{M}$. This evolution is given by the linear operator defined by[42]

$$(Uf)(X) = f(\Phi X) \tag{2.5}$$

We consider that the functional space $\{f(X)\}$ is a Banach or Fréchet space where the evolution operator can be written as an integral operator whose kernel is a distribution

$$(U^n f)(X) = \int \delta(\Phi^n X - Y) f(Y)\, dY \tag{2.6}$$

where δ is the two-dimensional Dirac distribution.

We expect that, for hyperbolic mappings, the correlation function between two observables f and g will decay like

$$C(n) \equiv \langle gU^n f \rangle = \sum_\nu (c_\nu^{(0)} + c_\nu^{(1)}|n| + \cdots + c_\nu^{(m_\nu)}|n|^{m_\nu}) e^{-\gamma_\nu \tau |n|} \tag{2.7}$$

The γ's are the decay or relaxation rates, which are intrinsic to the system and which we want to determine. They may have an imaginary part, but their real part is always nonnegative. By time-reversal symmetry, $C(n) = C(-n)$.

As a consequence of (2.7), the spectral function defined by the Fourier transform of the correlation function admits two families of poles at[32]

$$\omega = \pm i\gamma_\nu + \frac{2\pi m}{\tau} \qquad (m \in \mathbf{Z}) \tag{2.8}$$

because the spectral function is defined by a sum for time running from $-\infty$ to $+\infty$. However, in the decay of the correlation function at positive or negative times, only poles out of one of both families contribute because of the mixing property. Moreover, the multiplicity of the poles (2.8) is m_ν.

Several recent works have shown how the decay rates can be calculated from the complex zeros of the Fredholm determinant of the evolution operator according to[28,30,43]

$$0 = \det(I - yU) = \exp - \sum_{n=1}^{\infty} \frac{y^n}{n} \operatorname{Tr} U^n \tag{2.9}$$

The zeros $\{y_\nu\}$ of this determinant are identified with the eigenvalues of U according to

$$\frac{1}{y_\nu} = e^{-\gamma_\nu \tau}, \qquad \gamma_\nu = \frac{1}{\tau} \ln y_\nu \tag{2.10}$$

which give the decay rates $\{\gamma_\nu\}$ appearing in (2.7). The trace of U^n is defined from the kernel appearing in (2.6). The trace is then transformed into a sum over the fixed points of Φ^n using a well-known property of the Dirac distribution

$$\operatorname{Tr} U^n \equiv \int dX\, \delta(\Phi^n X - X) = \sum_{X = \Phi^n X} |\det[J^{(n)}(X) - I]|^{-1} \tag{2.11}$$

In (2.11), we denote by

$$J^{(n)}(X) = \frac{\partial \Phi^n}{\partial X}(X) \tag{2.12}$$

the Jacobian matrix of the mapping Φ^n at the fixed point X.

Since the mapping is assumed to be hyperbolic, each fixed point possesses one unstable and one stable eigenvalue. Working in the local coordinates around each fixed point, we expand the determinant of Eq. (2.11) into a Taylor series

$$|\det[J^{(n)}(X)-I]|^{-1}=\frac{1}{|\Lambda_u^{(n)}|}+\frac{2}{|\Lambda_u^{(n)}|\Lambda_u^{(n)}}+\frac{3}{|\Lambda_u^{(n)}|\Lambda_u^{(n)2}}+\frac{4}{|\Lambda_u^{(n)}|\Lambda_u^{(n)3}}+\cdots \tag{2.13}$$

Replacing the results into (2.9), the Fredholm determinant can be rewritten as a product of Ruelle's zeta functions[43]

$$\det(I-yU)=\frac{1}{\zeta_1(y)}\frac{1}{\zeta_2(y)^2}\frac{1}{\zeta_3(y)^3}\frac{1}{\zeta_4(y)^4}\cdots \tag{2.14}$$

defined as[28]

$$\zeta_\beta(y)\equiv\exp\sum_{n=1}^{\infty}\frac{y^n}{n}\sum_{X=\Phi^n X}\frac{1}{|\Lambda_u^{(n)}(X)|\Lambda_u^{(n)}(X)^{\beta-1}} \tag{2.15}$$

For systems which are uniformly hyperbolic, we have $\Lambda_u^{(n)}(X)=\Lambda^n$, where Λ is the uniform stretching factor. Furthermore, the model that we shall describe in the next section possesses a symbolic dynamics equivalent to a topological Markov chain. Its trajectories are in one-to-one correspondence with bi-infinite sequences of symbols. A transition matrix A composed of 0's and 1's rules the way the symbols follow each other in these bi-infinite symbolic sequences.[39,40] The number of fixed points of Φ^n, which we denote by $\mathcal{N}_n$, is then given by the standard trace of the topological transition matrix[39]

$$\mathcal{N}_n=\mathrm{Tr}\,A^n \tag{2.16}$$

The zeta function becomes

$$\zeta_\beta(y)=\exp\sum_{n=1}^{\infty}\frac{\mathcal{N}_n}{n}\left(\frac{y}{\Lambda^\beta}\right)^n \tag{2.17}$$

We obtain finally

$$\zeta_\beta(y)=\frac{1}{\det(I-y\Lambda^{-\beta}A)} \tag{2.18}$$

The calculation of the zeta function then reduces to the eigenvalue problem for the transition matrix A. We emphasize that this simple result holds only for uniformly hyperbolic systems like the multibaker chain.

According to the Perron–Frobenius theorem,[44] if the nonnegative matrix A is irreducible and aperiodic, it possesses a simple and positive eigenvalue which is larger than or equal to the moduli of all the others. The corresponding eigenvector and adjoint eigenvector have positive elements. We have thus the eigenvalues equations

$$A|\varphi_m\rangle = \chi_m|\varphi_m\rangle \tag{2.19}$$

$$\langle\tilde{\varphi}_m|A = \chi_m\langle\tilde{\varphi}_m| \tag{2.20}$$

for $m = 1, 2,..., M$ and the eigenvalues are ordered like

$$\chi_1 \geqslant |\chi_2| \geqslant |\chi_3| \geqslant \cdots \geqslant |\chi_M| \tag{2.21}$$

with $\chi_1 > 0$.

If we know the eigenvalues of the matrix A, the Fredholm determinant is then given by the infinite product

$$\det(I - yU) = \prod_{m=1}^{M} \left(1 - \frac{\chi_m}{\Lambda} y\right)\left(1 - \frac{\chi_m}{\Lambda^2} y\right)^2 \left(1 - \frac{\chi_m}{\Lambda^3} y\right)^3 \cdots \tag{2.22}$$

For each factor labeled by m, the infinite product shows absolute convergence for every value of y since

$$\sum_{\beta=1}^{\infty} \frac{\beta}{\Lambda^\beta} < \infty \tag{2.23}$$

because $\Lambda > 1$. As a consequence, the zeros of the factors, i.e.,

$$y_{m,\beta} = \frac{\Lambda^\beta}{\chi_m}, \qquad m = 1, 2, 3,..., M; \quad \beta = 1, 2, 3,... \tag{2.24}$$

are also zeros of the infinite product (2.22). Whereupon the decay rates of our dynamical system are given by

$$\gamma_{m,\beta} \equiv \frac{1}{\tau} \ln y_{m,\beta} = \frac{1}{\tau} \ln \frac{\Lambda^\beta}{\chi_m} \tag{2.25}$$

The multiplicity of $\gamma_{m,\beta}$ is β. The solutions (2.25) are the final solutions of our eigenvalue problem (2.9).

A crucial observation that will be made in the following is that the stretching factor Λ is always larger than or equal to the largest eigenvalue of the matrix A,

$$\Lambda \geqslant \chi_1 \tag{2.26}$$

Although (2.26) appears here as an assumption, we shall see that this inequality is satisfied in the examples of the following sections. (2.26) results from the geometry of the folding mechanism induced by stretching in phase space. The inequality (2.26) says that the number of periodic orbits cannot grow at a rate which is faster than provided by the stretching mechanism. This condition is generally satisfied in deterministic and uniformly hyperbolic mappings. Because of (2.26), all the decay rates (2.25) have a positive real part.

Two cases arise. In the first case, the system is open and particles can escape from the vicinity of the selected fixed points of Φ^n, which have been used in the preceding calculation. In this case, the slowest decay rate

$$\gamma \equiv \gamma_{1,1} = \frac{1}{\tau} \ln \frac{\Lambda}{\chi_1} \tag{2.27}$$

is a nonvanishing real number which gives the escape rate. As we shall show later, the selected trajectories then form a fractal repeller of trapped trajectories.[41]

In the second case, the system is bounded: no trajectory escapes, so that $\Lambda = \chi_1$ and the escape rate vanishes. The resonance (2.27) then turns into the eigenvalue 1 of the evolution operator corresponding to constant eigenfunction.[11] The relaxation appearing in the mixing property will then be dominated by the second slowest decay rate, which is given in general by

$$\gamma_{2,1} = \frac{1}{\tau} \ln \frac{\Lambda}{\chi_2} \tag{2.28}$$

2.3. Invariant Probability Measure and Its Characteristic Quantities

Associated with the leading resonance is an invariant probability measure on the whole phase space for bounded systems when $\Lambda = \chi_1$ or on the fractal repeller. The invariant measure is constructed as a probabilistic Markov chain on the symbolic dynamics of alphabet $\mathscr{A}$. The corresponding transition matrix $\Pi_{\alpha\beta}$ is based on the topological transition matrix $A_{\alpha\beta}$. The matrix $\Pi_{\alpha\beta}$ must satisfy

$$\sum_{\beta} \Pi_{\alpha\beta} = 1, \qquad \alpha, \beta \in \mathscr{A} \tag{2.29}$$

The invariant probability measure is then the stationary measure with respect to $\Pi_{\alpha\beta}$, i.e.,

$$\sum_{\alpha} \pi_\alpha \Pi_{\alpha\beta} = \pi_\beta, \qquad \text{with} \quad \sum_{\alpha} \pi_\alpha = 1 \tag{2.30}$$

These conditions are satisfied for[8,39]

$$\Pi_{\alpha\beta}=\frac{A_{\alpha\beta}\varphi_\beta}{\chi_1\varphi_\alpha} \tag{2.31}$$

where $\{\varphi_\alpha\}$ are the components of the eigenvector $|\varphi_1\rangle$ of eigenvalue χ_1 in (2.9). π_α is given by

$$\pi_\alpha=\frac{\tilde{\varphi}_\alpha\varphi_\alpha}{\langle\tilde{\varphi}\,|\,\varphi\rangle} \tag{2.32}$$

taking the normalization into account. The invariant measure of a cylinder of length n is thus

$$\mu(\omega_0\omega_1\cdots\omega_{n-1})=\pi_{\omega_0}\Pi_{\omega_0\omega_1}\Pi_{\omega_1\omega_2}\cdots\Pi_{\omega_{n-2}\omega_{n-1}} \tag{2.33}$$

so that the dynamics on the repeller is isomorph in the sense of Ornstein[45] to a probabilistic Markov chain.

Kolmogorov-Sinai (KS) and topological entropies per unit time. Because the system is equivalent to a Markov chain, the KS entropy is given by

$$h_{\rm KS}=-\frac{1}{\tau}\sum_{\alpha,\beta}\pi_\alpha\Pi_{\alpha\beta}\ln\Pi_{\alpha\beta}=\frac{1}{\tau}\ln\chi_1=h_{\rm top} \tag{2.34}$$

Since the system is assumed to be uniformly hyperbolic, the KS entropy is equal to the topological entropy, which is defined as the rate of increase in the number (2.16) of periodic orbits with their period. $h_{\rm top}$ is thus given in terms of the largest eigenvalue χ_1 of the topological transition matrix A and the last equality of (2.34) results.

Ruelle's topological pressure. This quantity of the thermodynamic formalism is defined by[28]

$$P(\beta)\equiv\lim_{n\to\infty}\frac{1}{n\tau}\ln\sum_{\omega_0\cdots\omega_{n-1}}\Lambda(\omega_0\omega_1\cdots\omega_{n-1})^{-\beta} \tag{2.35}$$

in terms of the stretching factors along the itineracies $\omega_0\cdots\omega_{n-1}$ which are allowed by the topological transition matrix A. As a consequence of the uniform hyperbolicity, all stretching factors are equal to Λ^n, so that

$$P(\beta)=\lim_{n\to\infty}\frac{1}{n\tau}\ln(\langle 1|A^{n-1}|1\rangle\Lambda^{-n\beta})=\frac{1}{\tau}\ln\chi_1-\frac{\beta}{\tau}\ln\Lambda \tag{2.36}$$

where $|1\rangle$ denotes a vector with all its elements equal to one. An equivalent definition of the topological pressure is given by continuation of

the smallest zero $y_{1,\beta}$ of the Fredholm determinant to real numbers for the parameter β, i.e.,

$$P(\beta) = -\frac{1}{\tau} \ln y_{1,\beta} \tag{2.37}$$

which is identical to (2.36). The mean Lyapunov exponent is known to be obtained by deriving the pressure at $\beta = 1$,

$$\lambda = -P'(1) \tag{2.38}$$

so that (2.3) is recovered as expected from the uniform hyperbolicity. The escape rate (2.27) is given exactly by

$$\gamma = -P(1) \tag{2.39}$$

The KS entropy (2.34) is then the difference between the Lyapunov exponent and the escape rate[14,46]

$$h_{\mathrm{KS}} = \lambda - \gamma \tag{2.40}$$

which generalizes Pesin's formula to open systems.

Dimensions. Because of the uniform hyperbolicity, all the generalized dimensions[47] of the invariant set are equal to

$$D_q = 2d_q = 2\frac{\ln \chi_1}{\ln \Lambda}, \qquad \forall q \tag{2.41}$$

d_q is the partial dimension, i.e., the dimension of the intersections of a line with the stable or unstable manifolds. We find the Hausdorff dimension D_{H} at $q = 0$ equal to the information dimension D_{I} at $q = 1$. The repeller is thus a simple fractal, with a trivial multifractal spectrum.

Alternatively, the partial dimension d_{H} is also given by $P(d_{\mathrm{H}}) = 0$ according to Bowen's formula.[48] d_{I} is also given by Young's formula as the ratio of the KS entropy over the mean Lyapunov exponent.[49]

Equilibrium state. We observe that the repeller fills the whole phase space when $\Lambda = \chi_1$ since (2.41) is then equal to two. In that case, the transition matrix of the Markov chain becomes

$$P_{\alpha\beta} = \frac{1}{\Lambda} A_{\alpha\beta} \tag{2.42}$$

with the stationary probabilities $\{p_\alpha\}$ corresponding to the uniform distribution. In the following, we shall denote this measure by

$$\text{Prob}(\omega_0\omega_1\cdots\omega_{n-1}) = p_{\omega_0}P_{\omega_0\omega_1}P_{\omega_1\omega_2}\cdots P_{\omega_{n-2}\omega_{n-1}} \tag{2.43}$$

This invariant measure shall be referred to as the equilibrium state.

3. INFINITE CHAIN OF COUPLED BAKER MAPS

3.1. Definition of the Multibaker Map

We construct the multibaker mapping on an infinite chain of squares. The mapping is area-preserving. The phase space is a strip of unit height and extending indefinitely to the left and the right. The multibaker map is composed of two successive mappings Φ_1 and Φ_2, each of which acts over a time $\tau/2$, so that the multibaker map itself acts over a time τ (see Fig. 1).

The first map Φ_1 is composed of an infinite number of baker transformations acting on adjacent and nonintersecting squares of unit area. These squares are defined to be

$$S_1^{(k)} = \{(x, y): k - \tfrac{1}{2} \leqslant x < k + \tfrac{1}{2}; 0 \leqslant y < 1\} \tag{3.1}$$

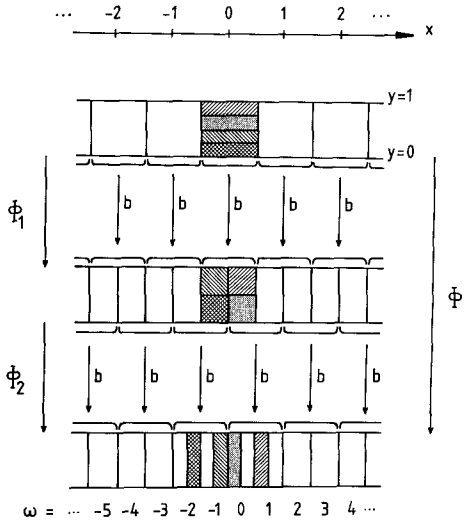

Fig. 1. Multibaker mapping Φ along an infinite chain. Φ is the composition of Φ_1 followed by Φ_2. b denotes an elementary baker transformation acting on a single square of the chain by a vertical stretching toward positive y, horizontal cutting at $y = 1$, and gluing at the right-hand side.

On each of these squares, a baker transformation acts with vertical stretching, horizontal cutting, and gluing of the upper half to the right-hand side of the lower half:

$$\Phi_1(x, y) = \begin{cases} (x/2 + k/2 - \frac{1}{4}, 2y) & k - \frac{1}{2} \leqslant x < k + \frac{1}{2}, \quad 0 \leqslant y < \frac{1}{2} \\ (x/2 + k/2 + \frac{1}{4}, 2y - 1) & k - \frac{1}{2} \leqslant x < k + \frac{1}{2}, \quad \frac{1}{2} \leqslant y < 1 \end{cases} \tag{3.2}$$

for all k. The second mapping Φ_2 acts on the squares which are shifted by 1/2 to the left with respect to the squares (3.1), namely

$$S_2^{(k)} = \{(x, y): k \leqslant x < k + 1; 0 \leqslant y < 1\} \tag{3.3}$$

On these squares, the second mapping Φ_2 performs similar baker transformations as Φ_1 so that

$$\Phi_2(x, y) = \begin{cases} (x/2 + k/2, 2y) & k \leqslant x < k + 1, \quad 0 \leqslant y < \frac{1}{2} \\ (x/2 + k/2 + \frac{1}{2}, 2y - 1) & k \leqslant x < k + 1, \quad \frac{1}{2} \leqslant y < 1 \end{cases} \tag{3.4}$$

for all k. The infinite multibaker transformation is then defined by the composition of the mapping Φ_1 followed by the mapping Φ_2. By inspection of Fig. 1, which shows how $\Phi = \Phi_2 \circ \Phi_1$ acts on a square, we obtain

$$\Phi(x, y) = \begin{cases} (x/4 + 3k/4 - \frac{5}{8}, 4y) & k - \frac{1}{2} \leqslant x < k + \frac{1}{2}, \quad 0 \leqslant y < \frac{1}{4} \\ (x/4 + 3k/4 - \frac{1}{8}, 4y - 1) & k - \frac{1}{2} \leqslant x < k + \frac{1}{2}, \quad \frac{1}{4} \leqslant y < \frac{1}{2} \\ (x/4 + 3k/4 + \frac{1}{8}, 4y - 2) & k - \frac{1}{2} \leqslant x < k + \frac{1}{2}, \quad \frac{1}{2} \leqslant y < \frac{3}{4} \\ (x/4 + 3k/4 + \frac{5}{8}, 4y - 3) & k - \frac{1}{2} \leqslant x < k + \frac{1}{2}, \quad \frac{3}{4} \leqslant y < 1 \end{cases} \tag{3.5}$$

for all k. We can verify that the infinite strip is mapped onto itself as expected from the global area-preserving property.

3.2. Hyperbolicity of the Multibaker Map

Locally, the mapping Φ is area-preserving because its Jacobian determinant equals one. The linear stability of its trajectories is given by considering its Jacobian matrix, which rules the evolution of the infinitesimal separations between neighboring trajectories,

$$\begin{pmatrix} \delta x_{n+1} \\ \delta y_{n+1} \end{pmatrix} = \begin{pmatrix} 1/4 & 0 \\ 0 & 4 \end{pmatrix} \begin{pmatrix} \delta x_n \\ \delta y_n \end{pmatrix} \equiv J \begin{pmatrix} \delta x_n \\ \delta y_n \end{pmatrix} \tag{3.6}$$

As a consequence, any trajectory $(\Phi^t X)$ is unstable of saddle type. The stable manifold of each periodic or nonperiodic trajectory is composed of segments which are parallel to the x axis, while the segments composing its unstable manifold are parallel to the y axis. Consequently, the infinite multibaker mapping is uniformly hyperbolic with a stretching factor $\Lambda = 4$, as described in Section 2.1. According to (2.3), the Lyapunov exponent of the multibaker is thus equal to

$$\lambda = \frac{1}{\tau} \ln 4 \tag{3.7}$$

3.3. The Inverse Mapping and Its Reduction to a 1D Map

Our purpose here is to show that the inverse mapping Φ^{-1} is reducible to a one-dimensional map for the x coordinate which appears to drive the other y coordinate, playing a passive role. A symbolic dynamics will emerge naturally from this construction.

Figure 2 shows how $\Phi^{-1} = \Phi_1^{-1} \circ \Phi_2^{-1}$ acts in the phase space. By inspection of the geometry, we obtain the equations

$$\Phi^{-1}(x, y) = \begin{cases} (4x - 3k - \frac{1}{2},\ y/4 + \frac{1}{2}) & k \leqslant x < k + \frac{1}{4}, \quad 0 \leqslant y < 1 \\ (4x - 3k - \frac{1}{2},\ y/4) & k + \frac{1}{4} \leqslant x < k + \frac{1}{2}, \quad 0 \leqslant y < 1 \\ (4x - 3k - \frac{5}{2},\ y/4 + \frac{3}{4}) & k + \frac{1}{2} \leqslant x < k + \frac{3}{4}, \quad 0 \leqslant y < 1 \\ (4x - 3k - \frac{5}{2},\ y/4 + \frac{1}{4}) & k + \frac{3}{4} \leqslant x < k + 1, \quad 0 \leqslant y < 1 \end{cases} \tag{3.8}$$

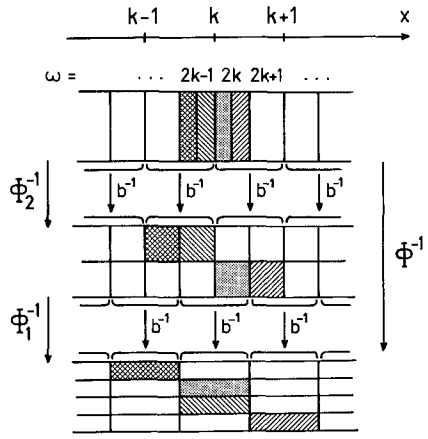

Fig. 2. The inverse mapping Φ^{-1} of the infinite multibaker mapping of Fig. 1.

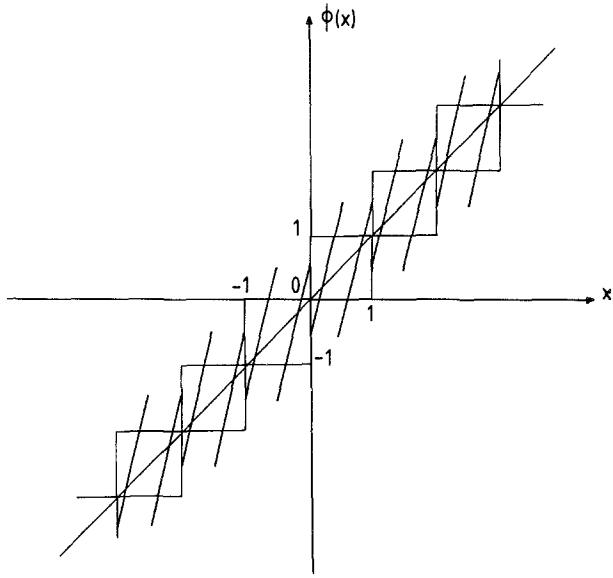

Fig. 3. One-dimensional map $\phi(x)$ ruling the motion of the x coordinate of a point under the inverse multibaker mapping Φ^{-1} of Fig. 2.

for all k. We observe that this inverse mapping acts on the x coordinate of the current point $X=(x, y)$ like the following one-dimensional mapping:

$$\phi(x)=\begin{cases}4x-3k-\frac{1}{2} & k\leqslant x<k+\frac{1}{2}\\ 4x-3k-\frac{5}{2} & k+\frac{1}{2}\leqslant x<k+1\end{cases} \tag{3.9}$$

(for all k) which is depicted in Fig. 3.

Let us note that the multibaker mapping is time-reversal symmetric. There exists a transformation T as in (2.4). T is given by an inversion along the diagonal of each square $S_1^{(k)}$ (see Fig. 4)

$$\mathrm{T}(x, y)=(y+k-\tfrac{1}{2}, x-k+\tfrac{1}{2}),\quad k-\tfrac{1}{2}\leqslant x<k+\tfrac{1}{2},\quad 0\leqslant y<1,\quad \forall k \tag{3.10}$$

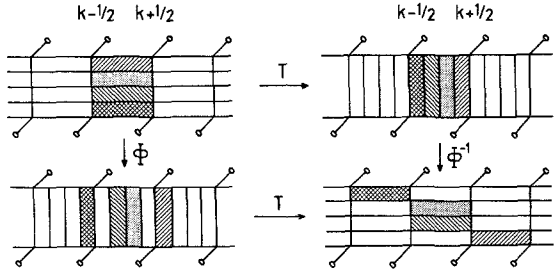

Fig. 4. Time-reversal transformation T and the geometrical proof of the invariance of Φ under T.

3.4. Symbolic Dynamics

According to the preceding result (3.9), we define the partition of the phase space into half square cells, labeling each cell as follows:

$$\begin{aligned} 2k-1 &\leftrightarrow \{(x, y):\ k-\tfrac{1}{2} \leqslant x < k,\ 0 \leqslant y < 1\} \\ 2k &\leftrightarrow \{(x, y):\ k \leqslant x < k+\tfrac{1}{2},\ 0 \leqslant y < 1\} \end{aligned} \tag{3.11}$$

where $2k-1$ is the left-hand half of the kth cell and $2k$ is its right-hand half. The symbolic dynamics is thus constructed on the infinite alphabet, $\omega_n \in \mathscr{A} = \mathbf{Z}$. This partition is generating in the sense that the trajectories are in one-to-one correspondence with the bi-infinite sequences on this alphabet obtained from the constraint that $2k-1$ and $2k$ can be followed with $(2k-2,\ 2k-1,\ 2k,\ 2k+1)$ only. The transition matrix of this topological Markov chain is thus

$$A = \begin{array}{c} \\ \vdots \\ -3 \\ -2 \\ -1 \\ 0 \\ 1 \\ 2 \\ \vdots \end{array} \begin{array}{c} \begin{array}{ccccccccccccc} \cdots & -5 & -4 & -3 & -2 & -1 & 0 & 1 & 2 & 3 & 4 & \cdots \end{array} \\ \begin{pmatrix} \ddots & \vdots & \vdots & \vdots & \vdots & \vdots & \vdots & \vdots & \vdots & \vdots & \vdots & \ddots \\ \cdots & & 1 & 1 & 1 & 1 & & & & & & \cdots \\ \cdots & & 1 & 1 & 1 & 1 & & & & & & \cdots \\ \cdots & & & & 1 & 1 & 1 & 1 & & & & \cdots \\ \cdots & & & & 1 & 1 & 1 & 1 & & & & \cdots \\ \cdots & & & & & & 1 & 1 & 1 & 1 & & \cdots \\ \cdots & & & & & & 1 & 1 & 1 & 1 & & \cdots \\ \ddots & \vdots & \vdots & \vdots & \vdots & \vdots & \vdots & \vdots & \vdots & \vdots & \vdots & \ddots \end{pmatrix} \end{array} \tag{3.12}$$

where the blanks stand for zeros.

Proof. (a) Because the cells of the partition are nonintersecting and fill the whole phase space, a unique symbolic sequence is given to each trajectory by recording the successive cells of the partition which are visited during its time evolution under Φ^t $(t \in \mathbf{Z})$ and from its initial condition (x, y).

(b) Let us suppose that the bi-infinite sequence $\underline{\omega}$ is compatible with the symbolic constraint (3.12) of the topological Markov chain. The initial condition (x, y) of the corresponding trajectory belongs to the cell ω_0. From Fig. 1, and because ω_1 is linked to ω_0 by the symbolic constraint, we see that the knowledge of ω_1 allows us to choose the only horizontal quarter of cell ω_0 to which (x, y) belongs. The main point here is the fact that there is no ambiguity in the choice between several quarters in cell ω_0. Similarly, we observe in Fig. 2 that ω_{-1} selects one and only one vertical

quarter in the cell ω_0. Therefore, the knowledge of $\omega_{-1} \cdot \omega_0 \omega_1$ restricts the set of initial conditions to a unique rectangle of area 1/32 inside ω_0. By recurrence, the cells $\omega_{-t} \cdots \omega_t$ form a unique sequence of rectangles of area $1/(2 \times 16^t)$ which are embedded into each other and which converges to a unique point which is the initial condition of the corresponding trajectory.

3.5. Reducing the Dynamics to a Lattice Cell

Exploiting the translational invariance of the dynamical system along the x axis, we can reduce the dynamics to a single cell of the lattice, together with a function on this reduced phase space which counts the jumps to the left or to the right. The whole dynamics along the chain can be decomposed into a dynamics inside a fictive cell of the lattice running along the lattice with the trajectory and composed with the jumping dynamics. Returning to Fig. 1, we see that the dynamics is reduced to a single cell of the lattice if the left-hand vertical quarter which belongs to the left-hand neighboring cell is placed on the right-hand blank quarter and similarly for the right-hand quarter (see Fig. 5). The reduced mapping Φ_r is thus

$$\Phi_r(x, y) = \begin{cases} (x/4 + \frac{3}{8}, 4y) & -\frac{1}{2} \leqslant x < +\frac{1}{2}, \quad 0 \leqslant y < \frac{1}{4} \\ (x/4 - \frac{1}{8}, 4y - 1) & -\frac{1}{2} \leqslant x < +\frac{1}{2}, \quad \frac{1}{4} \leqslant y < \frac{1}{2} \\ (x/4 + \frac{1}{8}, 4y - 2) & -\frac{1}{2} \leqslant x < +\frac{1}{2}, \quad \frac{1}{2} \leqslant y < \frac{3}{4} \\ (x/4 - \frac{3}{8}, 4y - 3) & -\frac{1}{2} \leqslant x < +\frac{1}{2}, \quad \frac{3}{4} \leqslant y < 1 \end{cases} \tag{3.13}$$

The jumping dynamics is obtained by the history of the trajectory from initial condition (x, y), $\Phi_r^t(x, y)$, counting the passages by the aforementioned lower and upper quarters. $I_{S_+}(X)$ and $I_{S_-}(X)$ denote the indicator functions of the cells defined by

$$\begin{aligned} S_+ &= \{(x, y): -\tfrac{1}{2} \leqslant x < +\tfrac{1}{2}, \tfrac{3}{4} \leqslant y < 1\} \\ S_- &= \{(x, y): -\tfrac{1}{2} \leqslant x < +\tfrac{1}{2}, 0 \leqslant y < \tfrac{1}{4}\} \end{aligned} \tag{3.14}$$

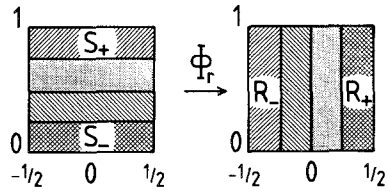

Fig. 5. Reduced cell mapping Φ_r. Here $S_\pm$ ($R_\pm$) denote the rectangles of the jump dynamics under Φ (Φ^{-1}).

A trajectory of the complete system is then reconstructed from the cell-reduced dynamics according to

$$x_t \equiv x(\Phi^t X) = x(\Phi_r^t X) + \sum_{m=0}^{t-1} I_{S_+}(\Phi_r^m X) - \sum_{m=0}^{t-1} I_{S_-}(\Phi_r^m X) \qquad (t>0) \quad (3.15)$$

As for the complete time-reversed mapping (3.8), the time-reversed reduced mapping acts on the x coordinate of the current point $X=(x, y)$ according to a one-dimensional mapping ϕ_r which is depicted in Fig. 6. An expression similar to (3.15) holds for negative times, replacing $S_\pm$ by the time-reversed domains $R_\pm$ shown in Fig. 5.

The preceding considerations lead us to introduce a velocity as the difference between the x coordinates of two successive points of a trajectory,

$$\begin{aligned} v(\Phi X) &= x(\Phi X) - x(X) = x(\Phi_r X) - x(X) + I_{S_+}(X) - I_{S_-}(X) \\ v(\Phi^{-1} X) &= x(\Phi^{-1} X) - x(X) = x(\Phi_r^{-1} X) - x(X) + I_{R_+}(X) - I_{R_-}(X) \end{aligned} \quad (3.16)$$

so that we have

$$x(X_t) = x(X_0) + \sum_{m=1}^{t} v(X_m) \quad (3.17)$$

Let us here mention that the reduced dynamics in a single lattice cell is a closed dynamical system of Bernoulli type on a symbolic dynamics with four symbols with probabilities $(\frac{1}{4}, \frac{1}{4}, \frac{1}{4}, \frac{1}{4})$. Consequently, it is ergodic, mixing, and of Kolmogorov type. Its Kolmogorov–Sinai entropy is $(1/\tau) \ln 4$, as expected.[11]

3.6. Diffusion

In this subsection, we take $\tau = 1$ unless otherwise stated. Diffusion takes place along the chain of baker transformations. We define the diffusion coefficient by

$$\mathscr{D} = \lim_{t \to \infty} \frac{1}{2t} \langle [x(\Phi^t X) - x(X)]^2 \rangle \quad (3.18)$$

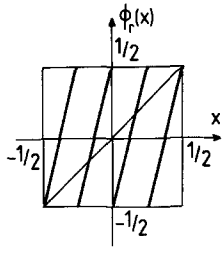

Fig. 6. One-dimensional mapping ϕ_r ruling the motion of the x coordinate of a point under the inverse reduced cell mapping Φ_r^{-1} of Fig. 5.

where $\langle \cdot \rangle$ denotes an average over an ensemble of initial conditions uniformly distributed over one lattice cell, which is the equilibrium measure of the cell-reduced dynamics.

The diffusion coefficient can be evaluated by different methods. The first one uses a direct evaluation of (3.18). Denoting $X_t \equiv \Phi_r^t X$, we obtain

$$\langle [x(X_t) - x(X_0)]^2 \rangle = \frac{t}{2} - \frac{1}{3}\left(1 - \frac{1}{4^t}\right) \tag{3.19}$$

so that

$$\mathscr{D} = \tfrac{1}{4} \tag{3.20}$$

If we suppose that the unit cells of the chain have a size a while an iteration is performed in a time τ, the diffusion coefficient acquires its physical units and reads $\mathscr{D} = (a^2)/(4\tau)$.

The Green–Kubo formula[50]

$$\mathscr{D} = \frac{C(0)}{2} + \sum_{m=1}^{\infty} C(m) \tag{3.21}$$

is of application for the present system, where $C(t)$ is the autocorrelation function of the velocity (3.16) given by

$$C(t) \equiv \langle v(\Phi^t X)\, v(X) \rangle = \frac{3}{8 \times 4^{|t|}} - \frac{1}{8}\delta_{t0} \tag{3.22}$$

so that $C(0) = 1/4$. Accordingly, we recover the diffusion coefficient (3.20). The velocity autocorrelation function is drawn in Fig. 7. The relaxation is here exponential and there is no long tail in this system.

The spectral function of the velocity autocorrelation function (3.22)

$$S(\omega) \equiv \sum_{n=-\infty}^{+\infty} e^{-i\omega n} C(n) = \frac{1}{2}\frac{7 + 2\cos\omega}{17 - 8\cos\omega} \tag{3.23}$$

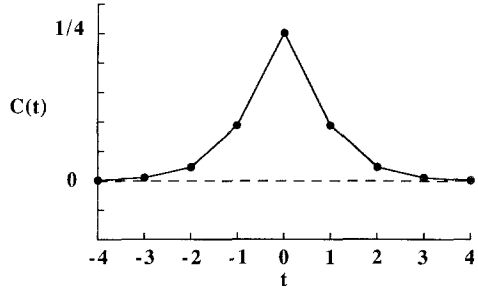

Fig. 7. Velocity autocorrelation function $C(t)$.

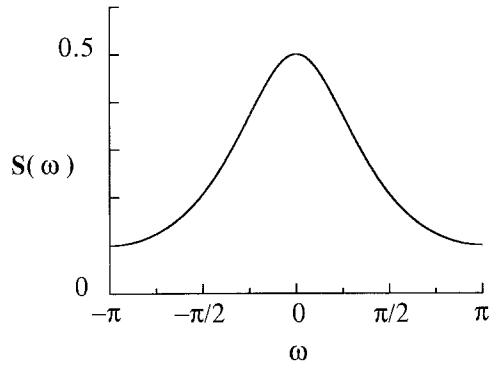

Fig. 8. Fourier transform of the velocity autocorrelation function. We observe the effect of the resonances at $\omega = \pm i \ln 4$.

is shown in Fig. 8. The diffusion coefficient is then given by the value of the power spectrum at zero frequency $\mathscr{D} = \frac{1}{2}S(0)$. We note that the spectral function presents two poles at $\omega = \pm i \ln 4$ in the cylinder $-\pi \leqslant \mathrm{Re}\,\omega < +\pi$ of the complex plane of the variable ω.

The existence of the diffusion coefficient for the multibaker chain and the mixing property for the lattice cell dynamics guarantees a central limit theorem for the random variable which is the x coordinate of the running particle:

$$\lim_{t\to\infty} \Pr\left\{\frac{x_t - x_0}{(2\mathscr{D}t)^{1/2}} < u\right\} = \frac{1}{(2\pi)^{1/2}} \int_{-\infty}^{u} e^{-y^2/2}\, dy \tag{3.24}$$

where Pr is the Lebesgue measure on the lattice cell.[51] This theorem is proved by methods developed by Doob[52] and Ibragimov.[53] Via a scaling limit, we infer from (3.24) that x_t follows a Brownian motion, in the sense that $\varepsilon x_{\varepsilon^2 t}$ converges to a Wiener process of diffusion constant $\mathscr{D}$ when $\varepsilon \to 0$.[25,54] These results justify the use of the phenomenological diffusion equation

$$\partial_t f = \mathscr{D}\, \partial_x^2 f \tag{3.25}$$

However, we shall see in next sections another approach where the classical Liouville dynamics is exactly solved, and which leads to a stronger correspondence between both dynamics based on the spectrum of complex resonances. This approach makes an explicit use of the detailed chaotic dynamics and, in this way, preserves the chaotic properties which are lost in the scaling limit $\varepsilon \to 0$. Indeed, the Wiener process generates erratic trajectories which are self-similar on arbitrary small scales. This feature can

be characterized by the entropy per unit time of the dynamical process with respect to a partition into cells of size ε, which is called an ε-entropy per unit time.[55,56] Because of its self-similarity, the ε-entropy of the Wiener process diverges like $h^{(\text{time})}(\varepsilon) \sim 1/\varepsilon^2$ as $\varepsilon \to 0$.[55,56] However, since the multibaker map is a deterministic hyperbolic system, its entropy per unit time with respect to an ε-partition has a supremum at the KS entropy per unit time, namely $\ln 4/\tau$. Since the trajectories of the multibaker map behave like those of a Wiener process only in the large-scale limit, we conclude that the ε-entropy per unit time of the multibaker map nevertheless decreases like $1/\varepsilon^2$ in the limit $\varepsilon \gg a$ after a crossover around $\varepsilon \sim a$. This behavior is depicted in Fig. 9. Consequently, there cannot be an isomorphism in the sense of Ornstein[45] between the Wiener process and the multibaker map because the entropy per unit time of the latter is overevaluated in the Wiener process at small $\varepsilon < a$. To avoid this fundamental problem common to each kinetic theory based on some scaling limit, we must preserve the chaotic character of deterministic systems, which is done in the theory developed in Section 2.

We summarize the preceding results as follows. We showed that the mean square displacement of the particles grows linearly with time, which defines the positive diffusion coefficient. We obtained a Green–Kubo formula for the diffusion coefficient in terms of the velocity autocorrelation function, which decays exponentially. As a consequence, the system presents no long tails, the power spectrum, i.e., the Fourier transform of the autocorrelation function, is continuous, and the dynamical fluctuations are Gaussian. These properties are to be compared to other systems with

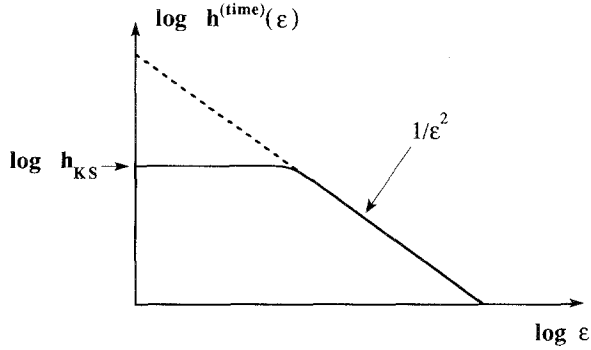

Fig. 9. ε-entropy per unit time for the infinite multibaker mapping. When ε is much larger than the lattice cell a, this decreases like $1/\varepsilon^2$ because the motion is Brownian on a large scale. The deterministic dynamics appears on small scales $\varepsilon \leqslant a$ where the finite KS entropy per unit time $(1/\tau) \ln 4$ is recovered. On small scales, the kinetic theory (dashed line) overestimates the entropy per unit time.

diffusion. In the Lorentz gas in a periodic array of hard disks fixed in the plane and with a finite horizon, such as the triangular lattice,[26] the velocity autocorrelation function is known to decay as a stretched exponential, so that this system presents no long tail, has a positive diffusion coefficient, and has Gaussian dynamical fluctuations.[25] Accordingly, in spite of several important differences, the multibaker chain presents some properties also found in the Lorentz gas with a finite horizon. Deterministic diffusion has also been studied in one-dimensional maps, where the present methods can be applied.[57–60]

To conclude this section, let us remark that the present multibaker chain is a model of space-time chaos as described in the introduction. Here $h_{KS} = \ln 4/\tau$ is the data accumulation rate necessary to reconstruct the trajectory of a single particle according to the Shannon–McMillan–Breiman theorem.[12] If a density of particles is present on the system, the data accumulation rate to follow many particles is proportional to the number ρ of particles per unit length. We can then define an entropy per unit time and unit length—as done previously by Goldstein *et al.*[16]—to describe the dynamical randomness of this system composed of many independent particles,

$$h^{(\text{time, length})} = \rho h_{KS} = \frac{\rho}{\tau} \ln 4 \tag{3.26}$$

The present model is thus able to sustain a process which is chaotic in space and time as in the hard-sphere gas. Although devoid of properties like temperature or heat conductivity, the multibaker chain is typical of space-time chaos.

4. FRACTAL REPELLERS IN THE CLOSED AND FINITE MULTIBAKER CHAIN

The purpose of this section is to show that fractal repellers appear in nonequilibrium problems for closed and isolated systems. We shall here consider a bounded variant of the infinite mapping of Section 3 in which particles cannot escape from a chain of length L. With this aim, a baker transformation acts on the two half-squares which remain at the two ends of the chain.

4.1. Definition of the System

The phase space is the strip of height 1 extending from $-1/2$ to $L + 1/2$ along the x axis. As in Section 3, the mapping is composed of two

submappings, Φ_1 followed by Φ_2. During the first map, a baker transformation with vertical stretching, horizontal cutting, and gluing at right hand acts on each of the $L+1$ squares (3.1) with $k=0, 1, 2,..., L$. The first mapping Φ_1 then takes the same form as (3.2), but here for $k=0, 1, 2,..., L$.

During the second mapping Φ_2, a baker transformation acts on the L squares (3.3) with $k=0, 1, 2,..., L-1$ which are shifted by 1/2 to the left with respect to the squares (3.1) and still contained in them. On the remaining part of phase space, namely on the two rectangles

$$\begin{aligned} \tilde{S}_2^{(-1)} &= \{(x, y): -\tfrac{1}{2} \leqslant x < 0; 0 \leqslant y < 1\} \\ \tilde{S}_2^{(L)} &= \{(x, y): L \leqslant x < L+\tfrac{1}{2}; 0 \leqslant y < 1\} \end{aligned} \tag{4.1}$$

the second mapping Φ_2 acts as a baker transformation, so that we can write

$$\Phi_2(x, y) = \begin{cases} (x/2 - \tfrac{1}{4}, 2y) & -\tfrac{1}{2} \leqslant x < 0, \quad 0 \leqslant y < \tfrac{1}{2} \\ (x/2, 2y-1) & -\tfrac{1}{2} \leqslant x < 0, \quad \tfrac{1}{2} \leqslant y < 1 \\ (x/2 + k/2, 2y) & k \leqslant x < k+1, \quad 0 \leqslant y < \tfrac{1}{2} \\ & k = 0, 1, 2,..., L-1 \\ (x/2 + k/2 + \tfrac{1}{2}, 2y-1) & k \leqslant x < k+1, \quad \tfrac{1}{2} \leqslant y < 1 \\ & k = 0, 1, 2,..., L-1 \\ (x/2 + L/2, 2y) & L \leqslant x < L+\tfrac{1}{2}, \quad 0 \leqslant y < \tfrac{1}{2} \\ (x/2 + L/2 + \tfrac{1}{4}, 2y-1) & L \leqslant x < L+\tfrac{1}{2}, \quad \tfrac{1}{2} \leqslant y < 1 \end{cases} \tag{4.2}$$

The finite multibaker transformation is then defined by the composition of the preceding mappings, $\Phi = \Phi_2 \circ \Phi_1$,

$$\Phi(x, y) = \begin{cases} (x/4 - \tfrac{3}{8}, 4y) & -\tfrac{1}{2} \leqslant x < +\tfrac{1}{2}, \quad 0 \leqslant y < \tfrac{1}{4} \\ (x/4 + 3k/4 - \tfrac{5}{8}, 4y) & k - \tfrac{1}{2} \leqslant x < k + \tfrac{1}{2}, \quad 0 \leqslant y < \tfrac{1}{4} \\ & k = 1, 2, 3,..., L \\ (x/4 + 3k/4 - \tfrac{1}{8}, 4y-1) & k - \tfrac{1}{2} \leqslant x < k + \tfrac{1}{2}, \quad \tfrac{1}{4} \leqslant y < \tfrac{1}{2} \\ & k = 0, 1, 2, 3,..., L \\ (x/4 + 3k/4 + \tfrac{1}{8}, 4y-2) & k - \tfrac{1}{2} \leqslant x < k + \tfrac{1}{2}, \quad \tfrac{1}{2} \leqslant y < \tfrac{3}{4} \\ & k = 0, 1, 2,..., L_i \\ (x/4 + 3k/4 + \tfrac{5}{8}, 4y-3) & k - \tfrac{1}{2} \leqslant x < k + \tfrac{1}{2}, \quad \tfrac{3}{4} \leqslant y < 1 \\ & k = 0, 1, 2,..., L-1 \\ (x/4 + 3L/4 + \tfrac{3}{8}, 4y-3) & L - \tfrac{1}{2} \leqslant x < L + \tfrac{1}{2}, \quad \tfrac{3}{4} \leqslant y < \tfrac{1}{2} \end{cases} \tag{4.3}$$

We can verify that the image of the domain covers the whole phase space as required (see Fig. 10). The mapping is uniformly hyperbolic with a stretching factor equal to 4.

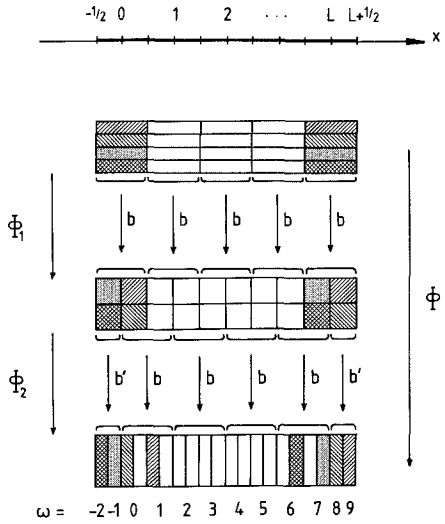

Fig. 10. Multibaker mapping Φ for a finite chain of length $L=4$. Φ is the composition of Φ_1 followed by Φ_2. b denotes an elementary baker transformation acting on a single square of the chain. Inside the chain, the mapping is the same as for the infinite chain. However, the particles are reinjected inside the chain at both ends where two baker transformations b' act on both half-squares.

The mapping Φ is area-preserving because its Jacobian determinant equals one everywhere.

As previously, the inverse mapping $\Phi^{-1}=\Phi_1^{-1}\circ\Phi_2^{-1}$ acts on the x coordinate of the current point like the one-dimensional mapping

$$\phi(x)=\begin{cases} 4x+\frac{3}{2} & -\frac{1}{2}\leqslant x<-\frac{1}{4} \\ 4x+\frac{1}{2} & -\frac{1}{4}\leqslant x<0 \\ 4x-3k-\frac{1}{2} & k\leqslant x<k+\frac{1}{2}, \quad k=0,1,2,\ldots,L-1 \\ 4x-3k-\frac{5}{2} & k+\frac{1}{2}\leqslant x<k+1, \quad k=0,1,2,\ldots,L-1 \\ 4x-3L-\frac{1}{2} & L\leqslant x<L+\frac{1}{4} \\ 4x-3L-\frac{3}{2} & L+\frac{1}{4}\leqslant x<L+\frac{1}{2} \end{cases} \tag{4.4}$$

which is depicted in Fig. 11 for $L=4$. According to this figure, we here define a partition of phase space as follows:

$$\begin{aligned} 2k &\leftrightarrow \{(x,y): k\leqslant x<k+\tfrac{1}{2}, 0\leqslant y<1\} \\ 2k+1 &\leftrightarrow \{(x,y): k+\tfrac{1}{2}\leqslant x<k+1, 0\leqslant y<1\} \end{aligned} \tag{4.5}$$

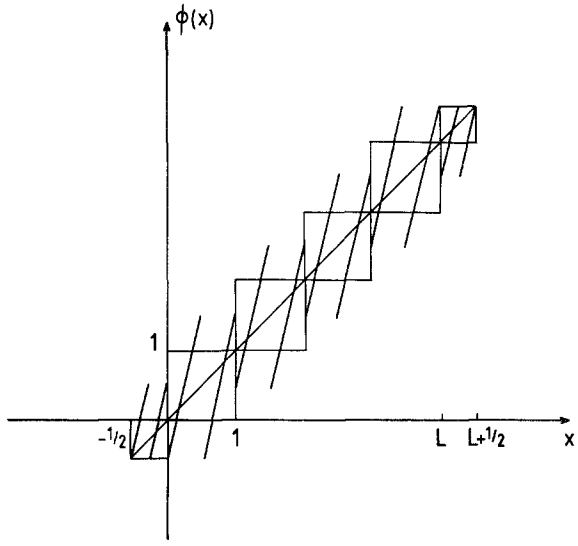

Fig. 11. One-dimensional mapping $\phi(x)$ ruling the motion of the x coordinate of a point under the inverse multibaker mapping Φ^{-1} of Fig. 10. We note that the stretching factor is everywhere equal to 4.

for $k=0, 1, 2,..., L-1$ and, furthermore, with the four rectangles of width 1/4,

$$\begin{aligned} -2 &\leftrightarrow \{(x, y): -\tfrac{1}{2} \leqslant x < -\tfrac{1}{4}, 0 \leqslant y < 1\} \\ -1 &\leftrightarrow \{(x, y): -\tfrac{1}{4} \leqslant x < 0, 0 \leqslant y < 1\} \\ 2L &\leftrightarrow \{(x, y): L \leqslant x < L + \tfrac{1}{4}, 0 \leqslant y < 1\} \\ 2L+1 &\leftrightarrow \{(x, y): L + \tfrac{1}{4} \leqslant x < L + \tfrac{1}{2}, 0 \leqslant y < 1\} \end{aligned} \tag{4.6}$$

The partition is generating in the sense that there is a one-to-one correspondence between the points of the trajectories of the system and the dotted bi-infinite sequences of the symbolic dynamics on the $2L+4$ symbols

$$\omega_n \in \mathscr{A} = \{-2, -1, 0, 1,..., 2L, 2L+1\} \tag{4.7}$$

The symbols ω_n themselves follow with constraints according to the $(2L+4) \times (2L+4)$ transition matrix of the topological Markov chain,

$$A_{\alpha\beta} = \begin{cases} 1 & \alpha = -2; \quad \beta = -2, -1, 0, 1 \\ & \alpha = 2k-1, 2k; \quad \beta = 2k-2, 2k-1, 2k, 2k+1 \quad (k = 0, 1, 2,..., L) \\ & \alpha = 2L+1; \quad \beta = 2L-2, 2L-1, 2L, 2L+1 \\ 0 & \text{otherwise} \end{cases} \tag{4.8}$$

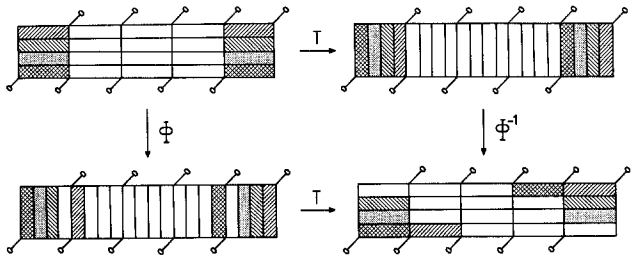

Fig. 12. Geometrical proof that the finite multibaker mapping Φ is invariant under the time-reversal transformation T.

For $L=4$, the transition matrix takes the form

$$A = \begin{array}{c} \\ -2 \\ -1 \\ 0 \\ 1 \\ 2 \\ 3 \\ 4 \\ 5 \\ 6 \\ 7 \\ 8 \\ 9 \end{array} \begin{array}{c} \begin{array}{cccccccccccc} -2 & -1 & 0 & 1 & 2 & 3 & 4 & 5 & 6 & 7 & 8 & 9 \end{array} \\ \left[\begin{array}{cccccccccccc} 1 & 1 & 1 & 1 & & & & & & & & \\ 1 & 1 & 1 & 1 & & & & & & & & \\ 1 & 1 & 1 & 1 & & & & & & & & \\ & & 1 & 1 & 1 & 1 & & & & & & \\ & & 1 & 1 & 1 & 1 & & & & & & \\ & & & & 1 & 1 & 1 & 1 & & & & \\ & & & & 1 & 1 & 1 & 1 & & & & \\ & & & & & & 1 & 1 & 1 & 1 & & \\ & & & & & & 1 & 1 & 1 & 1 & & \\ & & & & & & & & 1 & 1 & 1 & 1 \\ & & & & & & & & 1 & 1 & 1 & 1 \\ & & & & & & & & 1 & 1 & 1 & 1 \end{array}\right] \end{array} \tag{4.9}$$

As before, the mapping Φ is time-reversal symmetric under the involution (3.10) for $k=0, 1, 2,..., L$ (see Fig. 12).

4.2. Classical Resonances

A Koopman unitary operator corresponds to the mapping (4.3) for the closed and finite multibaker chain. This evolution operator has a continuous real spectrum because the mapping Φ is of Kolmogorov's type from the preceding considerations.[11] U has a single eigenvalue, which is 1, corresponding to a constant function on the phase space. When the evolution operator is extended, it acquires resonances which appear in the complex plane away from the unit circle. These resonances can be

calculated by the method of Section 2.2 based on the Fredholm determinant of U. Relations (2.18)–(2.25) apply here with the matrix A now given by (4.8)–(4.9).

We have the eigenvalue problem (2.19) for A with eigenvectors of the form

$$|\varphi\rangle = (u_{-1}, v_{-1}, u_0, v_0, u_1, v_1, ..., u_{L-1}, v_{L-1}, u_L, v_L)^T \tag{4.10}$$

The equations are

$$\begin{aligned} u_{-1} + v_{-1} + u_0 + v_0 &= \chi u_{-1} \\ u_{k-1} + u_{k-1} + u_k + v_k &= \chi v_{k-1} = \chi u_k \qquad (k = 0, 1, 2, ..., L) \\ u_{L-1} + v_{L-1} + u_L + v_L &= \chi v_L \end{aligned} \tag{4.11}$$

For the nonvanishing eigenvalues, we have that $u_k = v_{k-1}$ and the equations become

$$u_{k-1} + 2u_k + u_{k+1} = \chi u_k \qquad (k = 0, 1, 2, ..., L) \tag{4.12}$$

with the boundary conditions

$$\begin{aligned} u_{-1} &= u_0 \\ u_L &= u_{L+1} \end{aligned} \tag{4.13}$$

Assuming that the elements have the form

$$u_k = a \cos k\theta + b \sin k\theta \qquad (k = -1, 0, 1, 2, ..., L) \tag{4.14}$$

the eigenvalues are then given by

$$\chi = 2 + 2 \cos \theta \tag{4.15}$$

We obtain the eigenvalue condition

$$\sin[(L+1)\theta] = 0 \tag{4.16}$$

so that the angle θ takes the values

$$\theta_m = \frac{m\pi}{L+1} \qquad \text{for} \quad m = 0, 1, 2, ..., L+1 \tag{4.17}$$

Because the system is bounded, the eigenvalue $\chi = 4$ corresponding to the angle $\theta = 0$ is here the largest eigenvalue. We observe that the largest eigenvalue is thus equal to the stretching factor $\Lambda = 4$ of the system, so that the

important condition (2.26) is here satisfied. This equality arises because the present system is closed and thus has a vanishing escape rate.

According to (2.24)–(2.25), the decay rates are then exactly

$$\gamma_{m,\beta} = \frac{\beta}{\tau} \ln 4 - \frac{1}{\tau} \ln \left(2 + 2 \cos \frac{m\pi}{L+1} \right) \tag{4.18}$$

The decay modes ($m \geqslant 1$) are

$$u_k = v_{k-1} = \sin[(k+1)\theta] - \sin k\theta \qquad (k = -1, 0, 1, 2, \ldots, L+1) \tag{4.19}$$

and the eigenmode $m = 0$ is the constant function.

For a large multibaker chain, the family of slowest decay rates for $\beta = 1$ is

$$\gamma_{m,1} = \frac{1}{\tau} \ln \frac{2}{1 + \cos[m\pi/(L+1)]} = \mathscr{D} \left(\frac{m\pi}{L} \right)^2 + \mathcal{O}(L^{-3}) \tag{4.20}$$

where $\mathscr{D}$ is the diffusion coefficient calculated in Section 3. We observe that these relaxation rates that we exactly derived from the Liouville dynamics of the system approach the decay rates calculated from the phenomenological diffusion equation (3.25) solved for the boundary condition of zero flux at the ends of the chain,

$$\partial_x f = 0 \qquad \text{at} \quad x = 0, L \tag{4.21}$$

at any time. The general solution of (3.25) with (4.21) is

$$f(x, t) = \sum_{m=0}^{\infty} c_m \exp \left[-\mathscr{D} \left(\frac{m\pi}{L} \right)^2 t \right] \cos \frac{m\pi x}{L} \tag{4.22}$$

so that the decay rates obtained phenomenologically are

$$\gamma_m^{(\mathrm{ph})} = \mathscr{D} \left(\frac{m\pi}{L} \right)^2 \tag{4.23}$$

For a large system, the approximate decay rates (4.23) of the phenomenological equation converge to the exact ones (4.20). The approximate rates are slightly different from the exact ones by a small quantity of order L^{-3}. Besides this nice correspondence between the decay rates, we observe that the eigenvectors of the Liouville dynamics show the same shape as the corresponding phenomenological eigenmodes (see Fig. 13). This is one of the most important results of the present paper. Solving a phenomenological irreversible equation like the diffusion equation is a

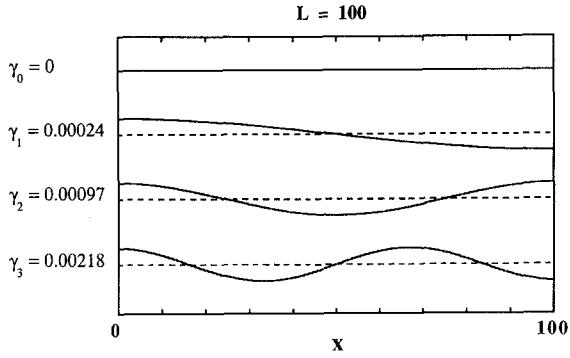

Fig. 13. Decay modes of the closed and finite multibaker mapping along a chain of length $L = 100$. They correspond to the family $\beta = 1$ ($m \geqslant 1$) of complex resonances. $m = 0$ is the constant eigenmode corresponding to the real eigenvalue 1 of the Koopmann operator. The values on the left column give the corresponding decay rates for $\tau = 1$.

cheap method to find the complex resonances of the Liouville dynamics. This result provides a more precise justification of the use of kinetic equations in nonequilibrium problems than the scaling-limit theories can provide. The property of dynamical chaos plays here a fundamental role in the existence of the complex resonances. Further comments about this correspondence at the level of the resonance spectrum will be given in the next section.

According to Section 2.3, the dynamics of the closed multibaker is isomorph to a probabilistic Markov chain. Because the eigenvector corresponding to the eigenvalue $\chi = 4$ is the constant vector, the invariant probability measure is (2.43) with the transition matrix and the stationary probability given by

$$P_{\alpha\beta} = \tfrac{1}{4} A_{\alpha\beta}$$
$$p_\alpha = \begin{cases} 1/(2L+2) & \alpha = 0, 1, 2, \ldots, 2L-1 \\ 1/(4L+4) & \alpha = -2, -1, 2L, 2L+1 \end{cases} \tag{4.24}$$

The topological pressure is here

$$P(\beta) = \frac{1-\beta}{\tau} \ln 4 \tag{4.25}$$

so that the Lyapunov exponent equals the KS entropy $\lambda = h_{\mathrm{KS}} = (1/\tau) \ln 4$. The invariant set fills the whole phase space with its Hausdorff dimension given by $D_{\mathrm{H}} = 2$. The invariant measure is the uniform distribution on $\mathscr{M}$ which defines the equilibrium thermodynamic state of the system.

4.3. A Fractal Repeller for Each Nonequilibrium State

Thermodynamic equilibrium is the stage of many dynamical processes, but they are dormant because time-reversed processes are equiprobable. To reveal these nonequilibrium dynamical processes, we must carry out observations over a finite time interval. As a consequence, we select trajectories which satisfy certain conditions imposed by the nature of the problem. Absorbing boundaries like those considered in first-passage problems in Kramers rate theory[61] are placed in phase space. Trajectories are eliminated as soon as they reach the absorbing boundaries. Since all trajectories of a chaotic system are unstable, most trajectories escape from the domain delimited by the boundaries, leaving only a set of trajectories of zero Lebesgue measure, which, in general, is a Cantor set. Accordingly, the absorbing boundaries and the development of a rate theory in a deterministic context, as done here, lead to the construction of a fractal repeller of trajectories satisfying the given nonequilibrium condition.

Several type of nonequilibrium conditions can be considered according to whether (1) one or several independent particles are present in the system, (2) the absorbing boundaries can be represented with strings containing one or several symbols of the symbolic dynamics, or (3) trajectories have to spend a given sojourn time in a domain.

In each case, a large-deviation formalism[62] can be developed to solve the nonequilibrium problem and calculate the escape rate from the corresponding fractal repeller, which is the ultimate goal of the theory.

In the following subsections, several examples of nonequilibrium conditions will be considered.

4.4. One-Particle, One-Symbol Nonequilibrium Conditions

4.4.1. Absorbing–Absorbing Boundaries. Suppose that we observe the diffusive transport out of a part of the multibaker chain. We place two absorbing boundaries at $x = k$ and $x = k + l$ and we select all the trajectories which stay forever in the domain

$$\mathscr{V} = \{k \leqslant x < k + l, 0 \leqslant y < 1\} \tag{4.26}$$

for given integers k and l such that $0 \leqslant k < l \leqslant L$. We shall show that the rate of escape out of this domain is related to the diffusion coefficient when l is large. The trajectories of the so-defined invariant set are in one-to-one correspondence with bi-infinite sequences composed of the symbols

$$\omega_n \in \{2k, 2k + 1, \ldots, 2k + 2l - 2, 2k + 2l - 1\} \tag{4.27}$$

These symbolic sequences must furthermore satisfy the transition rules of the matrix (4.9) of the topological Markov chain. Gathering these conditions, we define a new topological transition matrix

$$B_{\alpha\beta} \equiv \Delta_\alpha A_{\alpha\beta} \Delta_\beta \tag{4.28}$$

where

$$\Delta_\alpha = \begin{cases} 1 & \alpha = 2k, \ldots, 2k + 2l - 1 \\ 0 & \text{otherwise} \end{cases} \tag{4.29}$$

represents a projector onto the domain $\mathscr{V}$. The transition matrix B is a $2l \times 2l$ matrix which takes the following form when $k = 3$ and $l = 5$:

$$B = \begin{array}{c} \\ 6 \\ 7 \\ 8 \\ 9 \\ 10 \\ 11 \\ 12 \\ 13 \\ 14 \\ 15 \end{array} \begin{array}{c} \begin{array}{cccccccccc} 6 & 7 & 8 & 9 & 10 & 11 & 12 & 13 & 14 & 15 \end{array} \\ \left(\begin{array}{cccccccccc} 1 & 1 & & & & & & & & \\ 1 & 1 & 1 & 1 & & & & & & \\ 1 & 1 & 1 & 1 & & & & & & \\ & & 1 & 1 & 1 & 1 & & & & \\ & & 1 & 1 & 1 & 1 & & & & \\ & & & & 1 & 1 & 1 & 1 & & \\ & & & & 1 & 1 & 1 & 1 & & \\ & & & & & & 1 & 1 & 1 & 1 \\ & & & & & & 1 & 1 & 1 & 1 \\ & & & & & & & & 1 & 1 \end{array} \right) \end{array} \tag{4.30}$$

These conditions define a new topological Markov chain which is a subshift of the original symbolic dynamics.

The decay rates of the corresponding fractal repeller ($\mathscr{F}_l$) are calculated by solving the eigenvalue problem (2.19) with the matrix A replaced by B. The equiations are similar to (4.11)–(4.12) but with the boundary conditions

$$\begin{aligned} u_{-1} + u_0 &= 0 \\ u_l + u_{l+1} &= 0 \end{aligned} \tag{4.31}$$

replacing (4.13).

Using the same method as in Section 4.2, we obtain the decay rates given by Eq. (4.18) but here with L replaced by l and, more important, with the integer m running from $m = 1$ to $m = l$. The value $m = 0$ is not

allowed here because it is not compatible with the absorbing boundary conditions. For a large domain $\mathcal{V}$, the slowest decay rates have an expansion like (4.20) with the diffusion coefficient calculated in Section 3. As in Section 4.2, the exact relaxation rates of the Liouville dynamics of the system approach the decay rates calculated from the phenomenological diffusion equation (3.25), but now with absorbing boundaries, as a calculation similar to (4.22)–(4.23) shows. We also observe that the eigenvectors of the Liouville dynamics have the same shape as the corresponding phenomenological eigenmodes for absorbing boundaries (see Fig. 14). We conclude that the correspondence between the decay rates of the Liouville dynamics with those of the phenomenological equation can be performed here also in nonequilibrium problems.

The invariant measure is given by (2.31)–(2.33) and the Ruelle topological pressure is here

$$P(\beta)=\frac{1}{\tau}\ln\left(2+2\cos\frac{\pi}{l+1}\right)-\frac{\beta}{\tau}\ln 4 \tag{4.32}$$

so that the escape rate is

$$\gamma(\mathscr{F}_l)=-P(1)=\frac{1}{\tau}\ln\frac{2}{1+\cos[\pi/(l+1)]}=\mathscr{D}\left(\frac{\pi}{l}\right)^2+\mathcal{O}(l^{-3}) \tag{4.33}$$

The Lyapunov exponent is here also given by $(\ln 4)/\tau$, while the KS entropy per unit time now has a different value

$$h_{\mathrm{KS}}(\mathscr{F}_l)=\lambda(\mathscr{F}_l)-\gamma(\mathscr{F}_l)=\frac{1}{\tau}\ln\left(2+2\cos\frac{\pi}{l+1}\right) \tag{4.34}$$

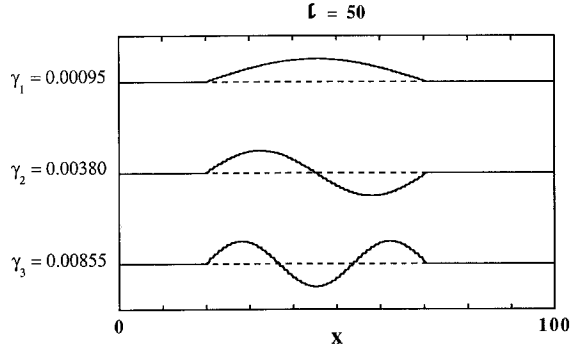

Fig. 14. Decay modes of the fractal repeller generated by two absorbing boundaries at $x=k=20$ and $x=k+l=70$ ($l=50$), together with their escape rate ($\tau=1$).

which equals the topological entropy. The Hausdorff dimension of the fractal repeller is here smaller than 2 (see Fig. 15)

$$D_H(\mathscr{F}_l) = \frac{1}{\ln 2} \ln\left(2 + 2\cos\frac{\pi}{l+1}\right) = 2 - \frac{1}{4\ln 2}\left(\frac{\pi}{l}\right)^2 + \mathcal{O}(l^{-3}) \quad (4.35)$$

and the selected trajectories form a set of zero Lebesgue measure, as required by the instability of the system. For l reaching the boundaries of the system L or for large l in a very large system L, the Hausdorff dimension converges to the value 2, meaning that the repeller fills the whole phase space in this limit.

We have the further important result that a relationship can be established between the diffusion coefficient and the difference between the Lyapunov exponent and the KS entropy of the nonequilibrium fractal $\mathscr{F}_l$ by using (4.33) together with (4.34). The diffusion coefficient can therefore be calculated from the characteristic quantities of chaos in the limit of a large system as follows:

$$\mathscr{D} = \lim_{l\to\infty} \left(\frac{l}{\pi}\right)^2 [\lambda(\mathscr{F}_l) - h_{KS}(\mathscr{F}_l)] \quad (4.36)$$

This formula has been the object of a recent letter,[9] where it was described in the context of the Lorentz gas of finite horizon. In the multibaker chain, this formula is proved with a control of the limit $l \to \infty$. We shall make further comments in Section 5.

4.4.2. Reflecting–Absorbing Boundaries. Another nonequilibrium problem is obtained by requiring that the particle remains forever in the domain

$$\mathscr{V} = \{-\tfrac{1}{2} \leqslant x < l; 0 \leqslant y < 1\} \quad (4.37)$$

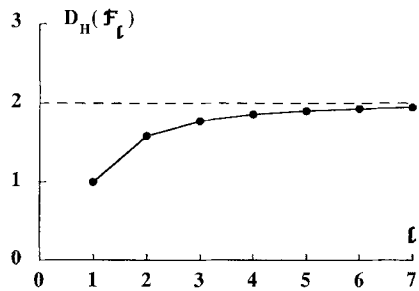

Fig. 15. Hausdorff dimension of the fractal repeller generated by two absorbing boundaries at $x = k$ and $x = k + l$ in the closed and finite multibaker mapping. As l increases, D_H converges to the phase space dimension 2.

with $l \leqslant L$. In this case $x = -1/2$ is a reflecting boundary, although $x = l$ is an absorbing boundary. The topological transition matrix is here defined by (4.28) with

$$\Delta_\alpha = \begin{cases} 1 & \alpha = -2, -1, 0, 1, \ldots, 2l-1 \\ 0 & \text{otherwise} \end{cases} \tag{4.38}$$

The transition matrix B is a $(2l+2)\times(2l+2)$ matrix ending like (4.9) at the left-hand boundary but like (4.30) at the right hand boundary. The boundary conditions for an eigenvector like (4.10) are now

$$\begin{aligned} u_{-1} &= u_0 \\ u_l + u_{l+1} &= 0 \end{aligned} \tag{4.39}$$

The scattering resonances of the present fractal repeller ($\tilde{\mathscr{F}}_l$) are

$$\gamma_{m,\beta} = \frac{\beta}{\tau} \ln 4 - \frac{1}{\tau} \ln \left(2 + 2 \cos \frac{(m+1/2)\pi}{l+1} \right) \tag{4.40}$$

The same remark as before applies here also about the correspondence with the phenomenological diffusion equation. In particular, the escape rate behaves like

$$\gamma(\tilde{\mathscr{F}}_l) = -P(1) = \frac{1}{\tau} \ln \frac{2}{1+\cos[\pi/(2l+2)]} = \mathscr{D} \left(\frac{\pi}{2l} \right)^2 + \mathscr{O}(l^{-3}) \tag{4.41}$$

Figure 16 shows how the reflecting boundary at $x = -1/2$ induces this doubling of the wavelength of the slowest eigenmode and the corre-

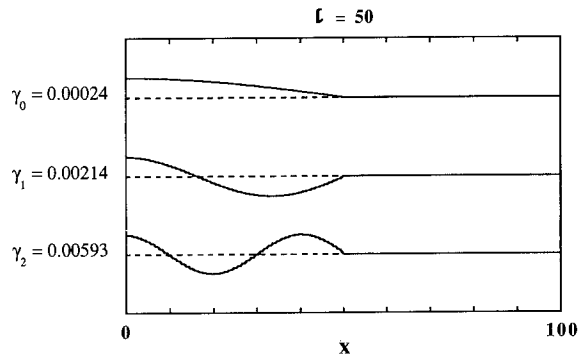

Fig. 16. Decay modes of the fractal repeller generated between the reflecting wall at $x = -1/2$ and an absorbing boundary at $x = l = 50$, together with their escape rate ($\tau = 1$). Comparison with Fig. 14 shows the doubling of the wavelength due to the replacement of an absorbing by a reflecting boundary.

sponding reduction by a factor four of the escape rate. The Hausdorff dimension of the fractal repeller is here

$$D_H(\tilde{\mathscr{F}}_l) = \frac{1}{\ln 2} \ln\left(2 + 2\cos\frac{\pi}{2l+2}\right) = 2 - \frac{1}{4\ln 2}\left(\frac{\pi}{2l}\right)^2 + \mathcal{O}(l^{-3}) \quad (4.42)$$

so that this fractal repeller behaves with l in a way similar to the preceding one.

4.5. One-Particle, Several-Symbol, Nonequilibrium Condition

When the absorbing boundaries imposed in the experiment do not fall at the border of the cells of the generating partition, several symbols are required to express the nonequilibrium constraint. In general, if the domain is expressible in terms of strings with n symbols, the topological transition matrix B will be

$$B_{\alpha_1\alpha_2\cdots\alpha_n,\beta_1\beta_2\cdots\beta_n} = \Delta_{\alpha_1\alpha_2\cdots\alpha_n} A_{\alpha_1\beta_1}\delta_{\beta_1\alpha_2} A_{\alpha_2\beta_2}\delta_{\beta_2\alpha_3}\cdots\delta_{\beta_{n-1}\alpha_n} A_{\alpha_n\beta_n}\Delta_{\beta_1\beta_2\cdots\beta_n} \quad (4.43)$$

The projector $\Delta_{\alpha_1\alpha_2\cdots\alpha_n}$ is defined by

$$\Delta_{\alpha_1\alpha_2\cdots\alpha_n} \equiv \begin{cases} 1 & \alpha_1\alpha_2\cdots\alpha_n \in \mathscr{A}^{(n)} \\ 0 & \text{otherwise} \end{cases} \quad (4.44)$$

where $\mathscr{A}^{(n)}$ is the set of strings of length n defining the admitted domain. $\delta_{\beta\alpha}$ is the usual Kronecker symbol. The matrix B is typically a $l^n \times l^n$ matrix which is much larger than in the preceding examples.

As a simple example, let us consider the trajectories which stay forever in the domain depicted in Fig. 17. The relaxation rates are

$$\gamma_{1,\beta} = \frac{\beta}{\tau}\ln 4 - \frac{1}{\tau}\ln(1+\sqrt{2}) \quad (4.45)$$

$$\gamma_{2,\beta} = \frac{\beta}{\tau}\ln 4 - \frac{1}{\tau}\ln(\sqrt{2}-1) - \frac{i\pi}{\tau} \quad (4.46)$$

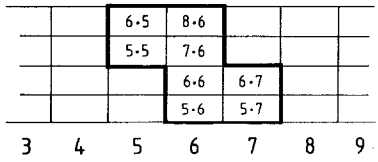

Fig. 17. Domain of the multibaker chain defined with strings of 2 symbols. Trajectories which are indefinitely trapped in this domain form a fractal repeller (see text).

with an example of a complex rate. The escape rate and the Hausdorff dimension are

$$\gamma \simeq 0.505 \frac{1}{\tau}, \qquad D_{\mathrm{H}} \simeq 1.272 \tag{4.47}$$

Because the fractal repeller extends over a small number of cells of the system, the escape rate gives a lifetime of the order of a microscopic time scale here. If we had considered a macroscopic domain, the lifetime would have been macroscopic.

4.6. One-Particle Condition on the Mean Sojourn Time in a Domain

For simplicity, $\tau = 1$ in this subsection. In the preceding examples, the trajectories were eliminated at the first iteration for which the chosen domain was left. Other nonequilibrium constraints can be envisaged where the particle is allowed to leave a domain for a while and to come back repetitively later, so that the mean sojourn time in $\mathscr{V}$ is a given fraction of the total time of the experiment.

Let $\mathscr{V}$ be a arbitrary domain in the phase space $\mathscr{M}$ and

$$I_{\mathscr{V}}(X) = \begin{cases} 1, & X \in \mathscr{V} \\ 0, & \text{otherwise} \end{cases} \tag{4.48}$$

be its indicator function. The fractal repeller is here defined as

$$\Upsilon(\alpha) = \left\{ X \in \mathscr{M} : \frac{1}{t} \sum_{n=0}^{t-1} I_{\mathscr{V}}(\Phi^n X) \to \alpha, \text{ for } t \to \infty \right\} \tag{4.49}$$

A similar problem was considered by Billingsley[12] for the dyadic expansion of real numbers of the unit interval as shown in the Appendix. The following developments generalize his results to large systems of statistical mechanics.

We introduce the set

$$\Upsilon_t(\alpha) = \left\{ X \in \mathscr{M} : \frac{1}{t} \sum_{n=0}^{t-1} I_{\mathscr{V}}(\Phi^n X) \in (\alpha, \alpha + d\alpha) \right\} \tag{4.50}$$

and we define a nonpositive function $F(\alpha)$ by[62]

$$\mathrm{Prob}\{\Upsilon_t(\alpha)\} = C(\alpha; t) e^{tF(\alpha)}\, d\alpha \tag{4.51}$$

where Prob is the equilibrium probability measure (2.43)–(4.24), i.e., the uniform distribution in the phase space $\mathscr{M}$. Here $C(\alpha; t)$ is a prefactor, which plays no essential role in the following considerations. From the definition (4.51), $F(\alpha)$ appears to be the escape rate from the set $\Upsilon(\alpha)$ of trajectories

$$\gamma = -F(\alpha) \tag{4.52}$$

A generating function $G(\beta)$ is defined by

$$G(\beta) \equiv \lim_{t \to \infty} \frac{1}{t} \ln \left\langle \exp \beta \sum_{n=0}^{t-1} I_{\Upsilon}(\Phi^n X) \right\rangle \tag{4.53}$$

were $\langle \cdot \rangle$ denotes the average over the equilibrium measure Prob. The generating function is related to $F(\alpha)$ by a Legendre transform according to

$$G(\beta) = F(\alpha) + \beta\alpha \tag{4.54}$$

where

$$\beta = -\frac{dF}{d\alpha} \qquad \text{or} \qquad \alpha = \frac{dG}{d\beta} \tag{4.55}$$

The topological pressure (2.35) of the set $\Upsilon(\alpha)$ of trajectories is defined by

$$P(q) = \lim_{t \to \infty} \frac{1}{t} \ln \sum_{\omega_0 \cdots \omega_{t-1} \in \Upsilon_t(\alpha)} 4^{-qt} A_{\omega_0\omega_1} A_{\omega_1\omega_2} \cdots A_{\omega_{t-2}\omega_{t-1}} \tag{4.56}$$

According to the definition (4.24) of the equilibrium measure, we have the relation

$$\text{Prob}\{\Upsilon_t(\alpha)\} \simeq \frac{2}{L+1} \sum_{\omega_0 \cdots \omega_{t-1} \in \Upsilon_t(\alpha)} 4^{-t} A_{\omega_0\omega_1} A_{\omega_1\omega_2} \cdots A_{\omega_{t-2}\omega_{t-1}} \tag{4.57}$$

up to a small correction of order $1/L^2$. The same sum as in (4.56) appears in (4.57). Comparing with (4.51), we obtain

$$P(q) = F(\alpha) + (1-q) \ln 4 \tag{4.58}$$

We emphasize that α in (4.58) is the parameter characterizing the set (4.49). The formula (4.58) should not be confused with a Legendre transform like (4.54) where α and β are conjugated variables. According to the formulas

(2.38)–(2.40), the Lyapunov exponent is $\lambda = \ln 4$, the escape rate is given by (4.52) as expected, the KS entropy is

$$h_{KS} = \ln 4 + F(\alpha) \tag{4.59}$$

and the Hausdorff dimension is

$$D_H = 2 + \frac{F(\alpha)}{\ln 2} \tag{4.60}$$

These relations are in agreement with the results by Billingsley[12] as shown in the Appendix.

Let us apply this formalism to an example where the domain $\mathscr{V}$ is expressible with one symbol. We take $\mathscr{V}$ as the left-hand half of the phase space $\mathscr{M}$, assuming that L is even,

$$\mathscr{V} = \left\{ -\frac{1}{2} \leqslant x < \frac{L}{2}; 0 \leqslant y < 1 \right\} \tag{4.61}$$

so that for $X = \cdots \omega_{-1} \cdot \omega_0 \omega_1 \cdots$,

$$I_{\mathscr{V}}(X) = \begin{cases} 1, & \omega_0 \in \{-2, -1, 0, 1, \ldots, L-1\} \\ 0, & \text{otherwise} \end{cases} \tag{4.62}$$

From the definition (2.43)–(4.24) of the equilibrium measure, the $G(\beta)$ function is summed as follows:

$$\begin{aligned} G(\beta) &= \lim_{n \to \infty} \frac{1}{n} \ln \sum_{\omega_0 \omega_1 \cdots \omega_{n-1}} \text{Prob}(\omega_0 \omega_1 \cdots \omega_{n-1}) \exp\left[\beta \sum_{m=0}^{n-1} I_{\mathscr{V}}(\omega_m) \right] \\ &= \lim_{n \to \infty} \frac{1}{n} \text{Tr}\, r\, R^{n-1} \end{aligned} \tag{4.63}$$

with

$$R_{\omega\tilde{\omega}} = P_{\omega\tilde{\omega}} e^{\beta I_{\mathscr{V}}(\tilde{\omega})} = \tfrac{1}{4} A_{\omega\tilde{\omega}} e^{\beta I_{\mathscr{V}}(\tilde{\omega})}, \tag{4.64}$$

$$r_{\omega\tilde{\omega}} = p_{\tilde{\omega}} e^{\beta I_{\mathscr{V}}(\tilde{\omega})} \tag{4.65}$$

Hence

$$G(\beta) = \ln \chi(\beta) \tag{4.66}$$

where $\chi(\beta)$ is the largest eigenvalue of the matrix R. For the case $L = 4$, the matrix R is given by

$$R = \begin{array}{c} \\ -2 \\ -1 \\ 0 \\ 1 \\ 2 \\ 3 \\ 4 \\ 5 \\ 6 \\ 7 \\ 8 \\ 9 \end{array} \begin{array}{c} \begin{array}{cccccccccccc} -2 & -1 & 0 & 1 & 2 & 3 & 4 & 5 & 6 & 7 & 8 & 9 \end{array} \\ \left[\begin{array}{cccccccccccc} w & w & w & w & & & & & & & & \\ w & w & w & w & & & & & & & & \\ w & w & w & w & & & & & & & & \\ & & w & w & w & w & & & & & & \\ & & w & w & w & w & & & & & & \\ & & & & w & w & s & s & & & & \\ & & & & w & w & s & s & & & & \\ & & & & & & s & s & s & s & & \\ & & & & & & s & s & s & s & & \\ & & & & & & & & s & s & s & s \\ & & & & & & & & s & s & s & s \\ & & & & & & & & s & s & s & s \end{array}\right] \end{array} \tag{4.67}$$

where

$$w = \tfrac{1}{4}\exp\beta \qquad \text{and} \qquad s = \tfrac{1}{4} \tag{4.68}$$

and the blanks stand for zeros. In order to determine the $G(\beta)$ function, we need to solve the eigenvalue problem for R. We assume an eigenvector of the form

$$|\varphi\rangle = (u_{-1}, v_{-1}, u_0, v_0, \ldots, u_L, v_L)^T \tag{4.69}$$

with $u_k = v_{k-1}$ for $\chi = 0$ and

$$\begin{aligned} u_k &= ae^{\xi k} + be^{-\xi k}, \qquad k = 0, 1, 2, \ldots, L/2 \\ u_k &= ce^{\eta k} + de^{-\eta k}, \qquad k = L/2, \ldots, L+1 \end{aligned} \tag{4.70}$$

with ξ and η two complex numbers to be found. The eigenvalue χ of R is then

$$\chi = \frac{e^{\beta}}{2}(1 + \cosh\xi) = \frac{1}{2}(1 + \cosh\eta) \tag{4.71}$$

The characteristic equation becomes

$$\tanh\frac{\xi}{2}\tanh\frac{\xi}{2}(L+1) + \tanh\frac{\eta}{2}\tanh\frac{\eta}{2}(L+1) = 0 \tag{4.72}$$

The coupled equations (4.71) and (4.72) have been solved numerically and the resulting $G(\beta)$ function is plotted in Fig. 18 together with its Legendre transform $F(\alpha)$. The asymptotic behaviors of these functions as well as their Taylor expansion around $\beta = 0$ and $\alpha = 1/2$, respectively, can be determined as follows.

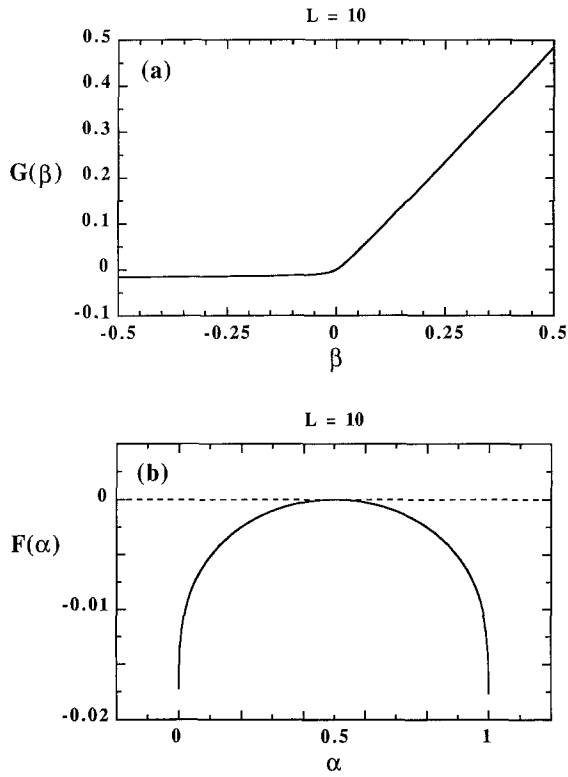

Fig. 18. (a) Generating function $G(\beta)$ of the mean value, the variance, and higher moments of the residence time in the left-hand half $(-1/2 \leqslant x < L/2)$ of the chain allowing exit and return from the domain; (b) the Legendre transform $F(\alpha)$ of $G(\beta)$ which gives minus the escape rate from the fractal repeller formed by the trajectories which spend a fraction α of their time in the left-hand half of the chain.

For $\beta \to +\infty$, the matrix elements of the left-hand side in (4.67) are so large that we can consider that the elements of the right-hand side of the chain are zero with respect to the others. In this limit, we should recover the eigenvalue problem solved in Section 4.4.2 with $l = L/2$. According to (4.71), ξ must then be imaginary and small while η is real and large

$$\xi \simeq i\theta, \qquad 4e^{\beta} \simeq e^{\eta} \tag{4.73}$$

Introducing these in (4.72), we obtain

$$\theta \simeq \frac{\pi}{L+2} \tag{4.74}$$

as expected. For large L, the eigenvalue is

$$\chi \simeq e^{\beta}\left[1-\frac{1}{4}\left(\frac{\pi}{L+2}\right)^2\right] \tag{4.75}$$

so that

$$G(\beta) \underset{\beta \to +\infty}{\simeq} \beta-\frac{1}{4}\left(\frac{\pi}{L+2}\right)^2 \tag{4.76}$$

Similarly, for $\beta \to -\infty$, the left-hand side gives negligible matrix elements in R, and we have

$$G(\beta) \underset{\beta \to -\infty}{\simeq} -\frac{1}{4}\left(\frac{\pi}{L+2}\right)^2 \tag{4.77}$$

When $\beta \simeq 0$ and positive, we assume here again that $\xi = i\theta$. Then (4.71) and (4.72) are expanded in Taylor series and solved to obtain

$$G(\beta)=\frac{\beta}{2}+\frac{1}{12}\left(L^2+2L+\frac{3}{2}\right)\beta^2+\mathcal{O}(\beta^3) \tag{4.78}$$

Its Legendre transform is

$$F(\alpha)=\frac{-3}{L^2+2L+3/2}\left(\alpha-\frac{1}{2}\right)^2+\cdots \tag{4.79}$$

We observe that $F(\alpha)$ reaches its maximum and vanishes at $\alpha = 1/2$, as expected, since the value $\alpha = 1/2$ corresponds to the frequency of visit of the left-hand part of the container at the thermodynamic equilibrium. The set of trajectories $\Upsilon(\alpha = 1/2)$ thus defines the equilibrium state and its escape rate is of course vanishing. On the other hand, the escape rate becomes nonvanishing as soon as α is taken with a value different from 1/2 and the corresponding set of trajectories is a fractal repeller. The $F(\alpha)$ function gives the escape rate from this repeller as explained before. The maximum escape rate is reached by the value of $F(\alpha)$ at the endpoints of its interval of definition

$$F(0)=F(1)=-\frac{1}{4}\left(\frac{\pi}{L+2}\right)^2+\mathcal{O}(L^{-3}) \tag{4.80}$$

The escape rates for this kind of nonequilibrium condition are thus typically of the order of $\mathcal{D}(\pi/L)^2$.

4.7. Fractal Repeller Generated in Trajectory Reconstruction

In this subsection, $\tau = 1$. We consider a further example of a fractal repeller generated by nonequilibrium constraints in the one-particle dynamics. We suppose that a measuring device observes the time evolution of the system. The measuring device has a finite resolution and resolves the system with a partition $\mathscr{P}$ of phase space $\mathscr{M}$ into cells labeled by integers $\sigma_n \in \{1, 2, ..., p\}$. The cells are here arbitrary without any reference to the generating partition considered in the previous examples. The trajectory $\Phi^t X$ from the initial condition X will produce a bi-infinite sequence

$$\underline{\sigma} = \cdots \sigma_{-2}\sigma_{-1} \cdot \sigma_0\sigma_1\sigma_2 \cdots \tag{4.81}$$

which appears as the recorded data from the measuring device. Once the observation has been made we would like to reconstruct the trajectory of the system from the observed data (4.81). We expect that this reconstruction will be possible only if the observation was carried out with a high enough resolution, i.e., if the partition is sufficiently fine. Otherwise, some ambiguity will arise in the reconstruction and we shall obtain a set of trajectories from the sequence $\underline{\sigma}$ rather than a single trajectory.

The question is thus the following. Given the partition $\mathscr{P}$, what is the Hausdorff dimension of the set of trajectories $\mathscr{F}_{\underline{\sigma}}$ which correspond to the recorded sequence $\underline{\sigma}$? If the partition $\mathscr{P}$ is generating, we know that a unique trajectory corresponds to $\underline{\sigma}$ and the Hausdorff dimension is then zero.

According to the Shannon–McMillan–Breiman theorem, we have that[12]

$$\text{Prob}(\sigma_0\sigma_1 \cdots \sigma_{t-1}) \sim \exp -th(\mathscr{P}) \tag{4.82}$$

for almost all the trajectories in $\mathscr{M}$. Here Prob is the equilibrium probability measure (2.43)–(4.24) and $h(\mathscr{P})$ is the entropy per unit time of the partition $\mathscr{P}$ with respect to the dynamical system. We see from (4.82) that the escape rate from the set $\mathscr{F}_{\underline{\sigma}}$ is precisely given by the entropy per unit time of the partition

$$\gamma(\mathscr{F}_{\underline{\sigma}}) = h(\mathscr{P}) \tag{4.83}$$

Because the system is uniformly hyperbolic, we always have

$$\lambda(\mathscr{F}_{\underline{\sigma}}) = \ln 4 \tag{4.84}$$

so that the KS entropy per unit time of the set $\mathscr{F}_{\underline{\sigma}}$ is

$$h_{\text{KS}}(\mathscr{F}_{\underline{\sigma}}) = \lambda(\mathscr{F}_{\underline{\sigma}}) - \gamma(\mathscr{F}_{\underline{\sigma}}) = \ln 4 - h(\mathscr{P}) \tag{4.85}$$

When the partition $\mathscr{P}$ is generating, then $h(\mathscr{P}) = \ln 4$ and $h_{KS}(\mathscr{F}_{\bar{\sigma}}) = 0$, since $\mathscr{F}_{\bar{\sigma}}$ contains then a single trajectory and is thus nonchaotic. For the generating partition also, the escape rate reaches its maximum, $\gamma(\mathscr{F}_{\bar{\sigma}}) = \ln 4$.

Let us now consider the case of an arbitrary partition $\mathscr{P}$. Because the system is uniformly hyperbolic, all the generalized dimensions are equal. According to Young's formula $D_I = 2h_{KS}/\lambda$,[49] we obtain the central result of this subsection,

$$D_H(\mathscr{F}_{\bar{\sigma}}) = D_I(\mathscr{F}_{\bar{\sigma}}) = 2 - \frac{h(\mathscr{P})}{\ln 2} \tag{4.86}$$

The set $\mathscr{F}_{\bar{\sigma}}$ is thus a fractal repeller. The Hausdorff dimension is depicted in Fig. 19 as a function of the entropy of the partition.

For a measuring device with a bad resolution, $h(\mathscr{P})$ is close to zero and the device can resolve the dynamics only into fractal sets with a dimension close to the phase space dimension. On the other hand, we see that the measuring device needs to have a data accumulation rate close to the KS entropy of the system, namely $h_{KS} = \ln 4$, to be able to resolve individual trajectories. There is a transition at h_{KS} where the Hausdorff dimension of the selected fractal set drops to zero. We can argue that this vanishing dimension is never reached because the partition of the measuring device never coincides exactly with the generating partition of the dynamics. In this way, a fractal dimension characterizes the resolving power of the measuring device observing a given dynamical system.

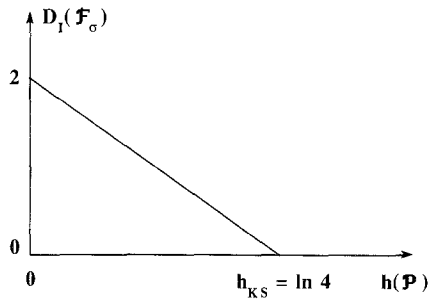

Fig. 19. Information or Hausdorff dimension of the fractal repeller formed by all the trajectories which visit the same sequence $\bar{\sigma}$ of cells of an arbitrary partition $\mathscr{P}$ of phase space, versus the entropy per unit time $h(\mathscr{P})$ of this partition $\mathscr{P}$. The information dimension vanishes when the partition $\mathscr{P}$ is the generating partition, in which case $h(\mathscr{P})$ is the KS entropy $h_{KS} = \ln 4$ of the multibaker mapping.

4.8. Nonequilibrium Conditions for the Many-Particle System

In the present subsection, we shall consider the problem of density fluctuations. We place in the system N independent particles and we require that, at each iteration, the number of particles in the left-hand half of the container is equal to M, which is in general different from $N/2$.

The phase space of the system is now

$$\underbrace{\mathcal{M} \otimes \mathcal{M} \otimes \cdots \otimes \mathcal{M}}_{N \text{ copies}} \tag{4.87}$$

of dimension $2N$. The trajectories of this dynamical system are in one-to-one correspondence with the bi-infinite sequences composed of N-uples of the symbols defined in the preceding sections:

$$\underline{\Omega} = \cdots \Omega_{-2}\Omega_{-1} \cdot \Omega_0\Omega_1\Omega_2 \cdots$$

$$= \begin{pmatrix} \cdots & \omega_{-2}^{(1)} & \omega_{-1}^{(1)} & \cdot & \omega_0^{(1)} & \omega_1^{(1)} & \omega_2^{(1)} & \cdots \\ \cdots & \omega_{-2}^{(2)} & \omega_{-1}^{(2)} & \cdot & \omega_0^{(2)} & \omega_1^{(2)} & \omega_2^{(2)} & \cdots \\ & \vdots & \vdots & & \vdots & \vdots & \vdots & \\ \cdots & \omega_{-2}^{(N)} & \omega_{-1}^{(N)} & \cdot & \omega_0^{(N)} & \omega_1^{(N)} & \omega_2^{(N)} & \cdots \end{pmatrix} \tag{4.88}$$

with

$$\omega_n^{(i)} \in \{-2, -1, 0, 2, \ldots, 2L, 2L+1\} \tag{4.89}$$

The invariant equilibrium measure is here

$$\text{Prob}(\Omega_0\Omega_1 \cdots \Omega_{n-1}) = \prod_{i=1}^{N} p_{\omega_0^{(i)}} P_{\omega_0^{(i)}\omega_1^{(i)}} P_{\omega_1^{(i)}\omega_2^{(i)}} \cdots P_{\omega_{n-2}^{(i)}\omega_{n-1}^{(i)}} \tag{4.90}$$

with (4.24), so that the KS entropy per unit time and the sum of positive Lyapunov exponents are both equal to

$$h_{\text{KS}} = \sum_{\lambda_i > 0} \lambda_i = \frac{N}{\tau} \ln 4 \tag{4.91}$$

We divide the chain into two halves and let $\mathscr{V}$ and $\mathscr{W}$ denote, respectively, the left- and right-hand halves:

$$\mathscr{V} = \{-1/2 \leqslant x < L/2; 0 \leqslant y < 1\} \tag{4.92}$$

$$\mathscr{W} = \{L/2 \leqslant x < L + 1/2; 0 \leqslant y < 1\} \tag{4.93}$$

for L even. $I_{\mathscr{V}}(X)$ and $I_{\mathscr{W}}(X)$ will denote the indicator functions of these domains.

Our nonequilibrium condition requires that, at each time t,

$$M_1 \leqslant \sum_{i=1}^{N} I_{\mathscr{V}}(\omega_t^{(i)}) \leqslant M_2 \qquad \text{with} \quad 1 \leqslant M_1 \leqslant M_2 \leqslant N \tag{4.94}$$

Because the particles are independent and because the domain $\mathscr{V}$ is described by an alphabet with $L+2$ symbols, the number of instantaneous states satisfying the above condition is

$$(L+2)^N \sum_{m=M_1}^{M_2} \binom{N}{m} \qquad \text{with} \quad \binom{N}{m} = \frac{N!}{m!\,(N-m)!} \tag{4.95}$$

out of the total number of states, which is $(2L+4)^N$. The fractal repeller defined by such a nonequilibrium condition is described by a topological Markov chain with a transition matrix

$$B_{\omega^{(1)}\omega^{(2)}\cdots\omega^{(N)},\,\tilde{\omega}^{(1)}\tilde{\omega}^{(2)}\cdots\tilde{\omega}^{(N)}} = \Delta_{\omega^{(1)}\omega^{(2)}\cdots\omega^{(N)}} A_{\omega^{(1)}\tilde{\omega}^{(1)}} A_{\omega^{(2)}\tilde{\omega}^{(2)}} \cdots A_{\omega^{(N)}\tilde{\omega}^{(N)}} \Delta_{\tilde{\omega}^{(1)}\tilde{\omega}^{(2)}\cdots\tilde{\omega}^{(N)}} \tag{4.96}$$

$\Delta_{\omega^{(1)}\cdots\omega^{(N)}}$ is the projector function which takes the value 1 on the states (4.95) and zero otherwise

$$\Delta_{\omega^{(1)}\omega^{(2)}\cdots\omega^{(N)}} = \sum_{\mathscr{X}_1\mathscr{X}_2\cdots\mathscr{X}_N \in \mathscr{G}} I_{\mathscr{X}_1}(\omega^{(1)})\, I_{\mathscr{X}_2}(\omega^{(2)}) \cdots I_{\mathscr{X}_N}(\omega^{(N)}) \tag{4.97}$$

where $\mathscr{G}$ is the set of

$$\sum_{m=M_1}^{M_2} \binom{N}{m} \tag{4.98}$$

allowed strings of N symbols $\mathscr{V}$ or $\mathscr{W}$ satisfying the nonequilibrium condition.

The decay rate from the nonequilibrium state is calculated from the eigenvalue equation

$$B|\Phi\rangle = \kappa|\Phi\rangle \tag{4.99}$$

where $|\Phi\rangle$ is a vector with a number of components equal to (4.95). To gain some insight into this problem, we make the following observation. Because of the structure (4.97) of the projector Δ, the matrix B can be rewritten

$$B_{\omega^{(1)}\omega^{(2)}\cdots\omega^{(N)},\,\tilde{\omega}^{(1)}\tilde{\omega}^{(2)}\cdots\tilde{\omega}^{(N)}} = \sum_{\mathscr{X}_1\mathscr{X}_2\cdots\mathscr{X}_N \in \mathscr{G}} \sum_{\tilde{\mathscr{X}}_1\tilde{\mathscr{X}}_2\cdots\tilde{\mathscr{X}}_N \in \mathscr{G}} A^{\mathscr{X}_1\tilde{\mathscr{X}}_1}_{\omega^{(1)}\tilde{\omega}^{(1)}} \cdots A^{\mathscr{X}_N\tilde{\mathscr{X}}_N}_{\omega^{(N)}\tilde{\omega}^{(N)}} \tag{4.100}$$

in terms of the four different matrices

$$A^{\mathscr{V}\mathscr{V}}, A^{\mathscr{V}\mathscr{W}}, A^{\mathscr{W}\mathscr{V}}, A^{\mathscr{W}\mathscr{W}} \tag{4.101}$$

defined by

$$A^{\mathscr{X}\tilde{\mathscr{X}}}_{\omega\tilde{\omega}} = I_{\mathscr{X}}(\omega)\, A_{\omega\tilde{\omega}}\, I_{\tilde{\mathscr{X}}}(\tilde{\omega}) \tag{4.102}$$

The matrix $A^{\mathscr{V}\mathscr{V}}$ is the matrix of the topological Markov chain for the nonequilibrium problem of Section 4.4.2 with a reflecting boundary at the left and an absorbing boundary at the middle of the chain (with $l = L/2$). The matrix $A^{\mathscr{W}\mathscr{W}}$ describes the symmetric condition with respect to the middle of the chain. However, the matrices $A^{\mathscr{V}\mathscr{W}}$ and $A^{\mathscr{W}\mathscr{V}}$ only contain a few nonvanishing elements near the middle of the chain.

The calculation of the escape rate appears as a formidable problem. We provide here a lower and an upper bound on it based on the following result of the Perron–Frobenius theorem, which says that the eigenvalue of a positive matrix like B is given by[44]

$$\kappa = \operatorname*{Max}_{|\Phi\rangle} \operatorname*{Min}_{\langle\omega^{(1)}\cdots\omega^{(N)}|} \frac{\langle\omega^{(1)}\cdots\omega^{(N)}|\, B\, |\Phi\rangle}{\langle\omega^{(1)}\cdots\omega^{(N)}|\,\Phi\rangle} \tag{4.103}$$

An upper bound on κ is given by the eigenvalue of the equilibrium state obtained by releasing all the nonequilibrium constraints, i.e., 4^N. A lower bound is obtained taking for $|\Phi\rangle$ the special vector

$$|\Phi\rangle = \underbrace{|\varphi^{\mathscr{V}}\rangle\cdots|\varphi^{\mathscr{V}}\rangle}_{m}\,\underbrace{|\varphi^{\mathscr{W}}\rangle\cdots|\varphi^{\mathscr{W}}\rangle}_{N-m} \tag{4.104}$$

where $|\varphi^{\mathscr{V}}\rangle$ and $|\varphi^{\mathscr{W}}\rangle$ are the eigenvectors of $A^{\mathscr{V}\mathscr{V}}$ and $A^{\mathscr{W}\mathscr{W}}$ corresponding to the largest eigenvalue calculated in Section 4.4.2 to be

$$\chi = 2 + 2\cos\frac{\pi}{L+2} \tag{4.105}$$

In the sum (4.100), we drop the terms for which $\mathscr{X}_i \neq \tilde{\mathscr{X}}_i$ to keep only the term with $\{\mathscr{X}_i\} = \{\tilde{\mathscr{X}}_i\} = \mathscr{V}\cdots\mathscr{V}\mathscr{W}\cdots\mathscr{W}$ in order to derive a minimum. The eigenvalue is thus bracketed in the interval

$$\chi^N \leqslant \kappa \leqslant 4^N \tag{4.106}$$

so that the escape rate is contained between the values

$$0 \leqslant \gamma \leqslant \frac{N}{\tau}\ln\frac{2}{1+\cos[\pi/(L+2)]} \simeq N\mathscr{D}\left(\frac{\pi}{L}\right)^2 \tag{4.107}$$

In the Appendix, a similar many-body problem is solved for the simple baker transformation. The conclusion is that fractal repellers also appear in the many-particle dynamics under nonequilibrium conditions.

4.9. The Multibaker Chain and Relaxation Toward Equilibrium

Due to the dynamical instability coming from the sensitivity to initial conditions, each trajectory of the multibaker chain is of saddle type with a positive Lyapunov exponent. In the preceding sections, we observed that nonequilibrium constraints in typical time-dependent experiments induce a selection of trajectories. The set of selected trajectories is in general nonempty and forms a fractal object in phase space because of the combination of hyperbolicity together with trapping, in particular, by periodic orbits. This fractal object defines what we called here a nonequilibrium state, which is characterized by a positive escape rate and, in general, a fractional Hausdorff dimension. The escape rate gives the rate of decay of the nonequilibrium state.

Since each trajectory is of saddle type, we remark that any nonequilibrium constraint inducing selection of a subset in phase space would give a dynamically unstable state. On the other hand, the equilibrium state composed of all trajectories in phase space weighted with the Liouville measure is stable since it fills the whole phase so that trajectories cannot escape somewhere else. By this property, the equilibrium state is unique and stable with respect to any other nonequilibrium state. This observation validates the second law of thermodynamics for the multibaker chain. We thus reach the following statement:

The dynamical system evolves spontaneously from each nonequilibrium fractal toward the stable equilibrium state.

This statement is weaker than the second law of thermodynamics because we do not mention here a monotonic increasing of the thermodynamic entropy in the system. The question have been debated recently by several authors[63–65] and shown to require the introduction of exactness in the sense of Mackey[63] or dynamically intrinsic coarse graining with the special partitions introduced by Nicolis and Nicolis.[65] In the present paper, we are not concerned with this question, but focus on direct relationships between the dynamical instability and the transport properties. We use the concept of KS entropy per unit time, which characterizes dynamical randomness in a way compatible with Hamiltonian or conservative dynamics. In open situations where nonequilibrium fractals are defined, the KS entropy and the Lyapunov exponent are related to the escape rate, which in turn is given by the transport properties. We are thus able to prove here the formula (4.36) for the nonequilibrium fractal $\mathscr{F}_l$ obtained

with two absorbing boundaries separated by a distance l (see Fig. 20). The transport coefficient emerges as a property of the large system arising from the limiting behavior of the escape rates on larger and larger domains. The formula (4.36) expresses explicitly this fact.

In the next section, we shall see that a fractal repeller naturally exists in large but open classical systems.

5. FRACTAL REPELLER IN THE OPEN AND FINITE MULTIBAKER CHAIN

5.1. Definition of the System

Systems which are studied in the laboratory are formed by a finite piece of material which is in contact through walls and probes to the laboratory and the observing devices. Let us idealize this situation by considering a finite chain of baker transformations from which the particle can enter or exit in free motion. The system in thus open and is the analogue for our simple model to the finite slab make up of a Lorentz lattice of hard-disk scatterers which was considered elsewhere.[9]

As in Section 3, the mapping is composed of two submappings, Φ_1 followed by Φ_2. The phase space is here again the strip of height 1 extending from $-\infty$ to $+\infty$ along the x axis. During the first map, a baker transformation with vertical stretching, horizontal cutting, and right-handed gluing acts on each of the $L+1$ squares (3.1) with $k=0, 1, 2,..., L$. On the remaining squares with $k=-1, -2, -3,...$ and $k=L+1, L+2,...$, the first mapping Φ_1 permutes the left-hand half with the right-hand, inducing a translational motion which is area-preserving but not hyperbolic. The first mapping can thus be written as follows:

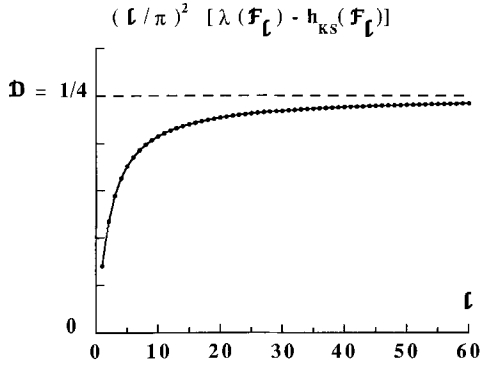

Fig. 20. Diagram showing how the diffusion constant is reached from the difference between the Lyapunov exponent and the KS entropy of the fractal repeller $\mathscr{F}_l$ generated by two absorbing boundaries separated by a distance l.

$$\Phi_1(x,y)=\begin{cases}(x+\frac{1}{2},\,y) & k-\frac{1}{2}\leqslant x<k,\quad 0\leqslant y<1\\ & k=-1,\,-2,\,-3,\ldots;\,L+1,\,L+2,\ldots\\ (x-\frac{1}{2},\,y) & k\leqslant x<k+\frac{1}{2},\quad 0\leqslant y<1\\ & k=-1,\,-2,\,-3,\ldots\,L+1,\,L+2,\ldots\\ (x/2+k/2-\frac{1}{4},\,2y) & k-\frac{1}{2}\leqslant x<k+\frac{1}{2},\quad 0\leqslant y<\frac{1}{2}\\ & k=0,\,1,\,2,\ldots,\,L\\ (x/2+k/2+\frac{1}{4},\,2y-1) & k-\frac{1}{2}\leqslant x<k+\frac{1}{2},\quad \frac{1}{2}\leqslant y<1\\ & k=0,\,1,\,2,\ldots,\,L\end{cases}\tag{5.1}$$

During the second mapping Φ_2, a baker transformation acts on the L squares (3.3) with $k=0,\,1,\,2,\ldots,\,L-1$. On the remaining part of the phase space, the second mapping Φ_2 permutes neighboring half squares two by two so that we can write

$$\Phi_2(x,y)=\begin{cases}(x+\frac{1}{2},\,y) & k\leqslant x<k+\frac{1}{2},\quad 0\leqslant y<1\\ & k=-1,\,-2,\,-3,\ldots;\,L,\,L+1,\,L+2,\ldots\\ (x-\frac{1}{2},\,y) & k+\frac{1}{2}\leqslant x<k+1,\quad 0\leqslant y<1\\ & k=-1,\,-2,\,-3,\ldots;\,L,\,L+1,\,L+2,\ldots\\ (x/2+k/2,\,2y) & k\leqslant x<k+1,\quad 0\leqslant y<\frac{1}{2}\\ & k=0,\,1,\,2,\ldots,\,L-1\\ (x/2+k/2+\frac{1}{2},\,2y-1) & k\leqslant x<k+1,\quad \frac{1}{2}\leqslant y<1\\ & k=0,\,1,\,2,\ldots,\,L-1\end{cases}\tag{5.2}$$

The finite multibaker transformation is then defined by the composition of the preceding mappings, $\Phi=\Phi_2\circ\Phi_1$,

$$\Phi(x,y)=\begin{cases}(x+1,\,y) & k-\frac{1}{2}\leqslant x<k,\quad 0\leqslant y<1\\ & k=\cdots,\,-3,\,-2,\,-1;\,L+1,\,L+2,\ldots\\ (x-1,\,y) & k\leqslant x<k+\frac{1}{2},\quad 0\leqslant y<1\\ & k=\cdots,\,-3,\,-2,\,-1;\,L+1,\,L+2,\ldots\\ (x/2-\frac{3}{4},\,2y) & -\frac{1}{2}\leqslant x<+\frac{1}{2},\quad 0\leqslant y<\frac{1}{2}\\ (x/2+L/2+\frac{3}{4},\,2y-1) & L-\frac{1}{2}\leqslant x<L+\frac{1}{2},\quad \frac{1}{2}\leqslant y<1\\ (x/4+3k/4-\frac{5}{8},\,4y) & k-\frac{1}{2}\leqslant x<k+\frac{1}{2},\quad 0\leqslant y<\frac{1}{4}\\ & k=1,\,2,\,3,\ldots,\,L\\ (x/4+3k/4-\frac{1}{8},\,4y-1) & k-\frac{1}{2}\leqslant x<k+\frac{1}{2},\quad \frac{1}{4}\leqslant y<\frac{1}{2}\\ & k=1,\,2,\,3,\ldots,\,L\\ (x/4+3k/4+\frac{1}{8},\,4y-2) & k-\frac{1}{2}\leqslant x<k+\frac{1}{2},\quad \frac{1}{2}\leqslant y<\frac{3}{4}\\ & k=0,\,1,\,2,\ldots,\,L-1\\ (x/4+3k/4+\frac{5}{8},\,4y-3) & k-\frac{1}{2}\leqslant x<k+\frac{1}{2},\quad \frac{3}{4}\leqslant y<1\\ & k=0,\,1,\,2,\ldots,\,L-1\end{cases}\tag{5.3}$$

We can verify that the image of the domain covers the whole phase space as required (see Fig. 21).

The mapping Φ is area-preserving because its Jacobian determinant equals one everywhere.

Trapped trajectories forming an invariant set of trajectories remaining foreover at finite distance exist only in the domain

$$\mathscr{V} = \{0 \leqslant x < L, 0 \leqslant y < 1\} \tag{5.4}$$

because the other part of phase space escapes to infinity under Φ or Φ^{-1} (see Fig. 21). As will appear later, the invariant set is a fractal contained in the domain $\mathscr{V}$. Most trajectories escape from $\mathscr{V}$ except the fractal set, which is of zero Lebesgue measure. In the domain $\mathscr{V}$, the dynamics is uniformly hyperbolic with stable manifolds of trapped trajectories composed of straight segments which are parallel to the x axis, while the unstable manifolds are parallel to the y axis. The stretching factor in the domain $\mathscr{V}$ is 4 as for the infinite multibaker transformation.

As before, the inverse mapping $\Phi^{-1} = \Phi_1^{-1} \circ \Phi_2^{-1}$ acts on the x coordinate of the current point $X = (x, y)$ like the one-dimensional mapping

$$\phi(x) = \begin{cases} 4x - 3k - \frac{1}{2} & k \leqslant x < k + \frac{1}{2}, \quad k = 0, 1, 2, \ldots, L-1 \\ 4x - 3k - \frac{5}{2} & k + \frac{1}{2} \leqslant x < k + 1, \quad k = 0, 1, 2, \ldots, L-1 \\ x + 1 & k \leqslant x < k + \frac{1}{2} \\ & k = \cdots, -4, -3, -2; L, L+1, L+2, \ldots \\ x - 1 & k + \frac{1}{2} \leqslant x < k + 1 \\ & k = \ldots, -3, -2, -1; L+1, L+2, \ldots \\ 2x + \frac{3}{2} & -1 \leqslant x < -\frac{1}{2} \\ 2x - L - \frac{3}{2} & L + \frac{1}{2} \leqslant x < L + 1 \end{cases} \tag{5.5}$$

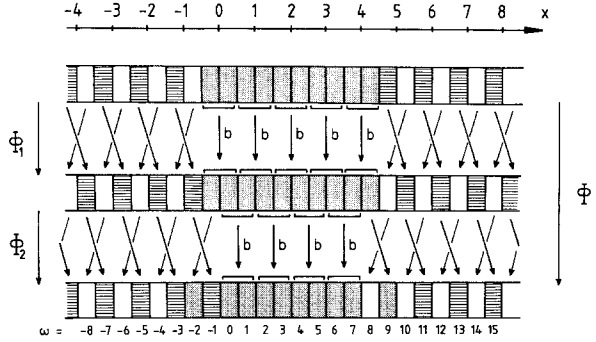

Fig. 21. Multibaker mapping Φ in its open version along the infinite phase space. Baker transformations (b) act on a portion of length l of phase space while translations act at left- and right-hand sides to model a flow of ingoing and outgoing particles to and from the scatterer. Φ is the composition of Φ_1 followed by Φ_2.

which is shown in Fig. 22 for $L=4$. We observe that fixed points for ϕ^n ($n=1, 2, 3,...$) can only exist in the interval $0 \leqslant x < L$. Accordingly, a partition of phase space into half-square cells is defined with the correspondence (4.5) for $k=0, 1, 2,..., L-1$ and, furthermore, with the two semi-infinite strips

$$\begin{aligned} - &\leftrightarrow \{(x, y): x<0, 0 \leqslant y<1\} \\ + &\leftrightarrow \{(x, y): L \leqslant x, 0 \leqslant y<1\} \end{aligned} \tag{5.6}$$

To each trajectory from the initial condition $X=(x, y)$ there corresponds a bi-infinite sequence of one of the following types:

$$\begin{aligned} &\text{Type I} && \xi^{\infty}\omega_1\omega_2\cdots\omega_n\zeta^{\infty} && \text{for} \quad n \geqslant 1 \\ &\text{Type II} && \xi^{\infty}\omega_1\omega_2\omega_3\cdots \\ &\text{Type III} && \cdots\omega_{-3}\omega_{-2}\omega_{-1}\zeta^{\infty} \\ &\text{Type IV} && \cdots\omega_{-3}\omega_{-2}\omega_{-1}\omega_0\omega_1\omega_2\omega_3\cdots \end{aligned} \tag{5.7}$$

with

$$\omega_n \in \{0, 1, 2, 3,..., 2L-2, 2L-1\} \qquad \text{and} \qquad \xi, \zeta \in \{+, -\} \tag{5.8}$$

The alphabet of this symbolic dynamics here contains $2L$ symbols. The

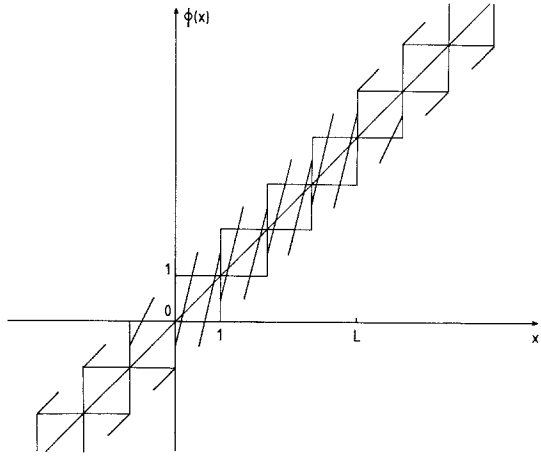

Fig. 22. One-dimensional mapping $\phi(x)$ ruling the motion of the x coordinate of a point under the inverse open multibaker mapping Φ^{-1} of Fig. 21.

symbols ω_n follow with constraints according to the topological transition matrix

$$A_{\alpha\beta}=\begin{cases}1 & \alpha=0;\ \beta=0,1\\ & \alpha=2k-1,2k;\ \beta=2k-2,2k-1,2k,2k+1\ \ (k=1,2,3,\ldots,L-1)\\ & \alpha=2L-1;\ \beta=2L-2,2L-1\\ 0 & \text{otherwise}\end{cases}\tag{5.9}$$

This $2L\times 2L$ transition matrix has the same form as the matrix (4.30) of the finite chain with two absorbing boundaries.

Trajectories of type I spend only a finite number of iterations in the domain $\mathscr{V}$. On the other hand, trajectories of type IV are trapped forever in the domain $\mathscr{V}$: they form the invariant set we shall call the fractal repeller, which is of vanishing Lebesgue measure because most trajectories are of type I. Trajectories of types II and III form the stable and unstable manifolds of the repeller, respectively. To each trajectory of type IV there correspond an infinite number of points, which we distinguish by a dot. The mapping Φ induces a shift operation to the left on the bi-infinite sequences. The trajectories of the repeller are in one-to-one correspondence with the bi-infinite sequences of type IV, so that the partition (4.5) is generating for the repeller.

Proof. (a) Assuming that the trajectories stay forever in $\mathscr{V}$ and because the cells of the partition are nonintersecting and cover this domain, a single symbolic sequence is given to each bi-infinite trapped trajectory by following its time evolution under $\Phi^t(t\in\mathbf{Z})$ from its initial condition. Once the trajectory exits $\mathscr{V}$, it necessarily escapes to infinity under Φ or Φ^{-1} so that such a trajectory is not bi-infinitely trapped, as assumed. (b) See Section 3.4.

The time-reversal transformation T for the mapping Φ is shown in Fig. 23. T is given by an inversion along the diagonal of each square $S_1^{(k)}$ $(k=0,1,2,\ldots,L)$. On the other squares $S_1^{(k)}$, T is given by an inversion along the diagonal followed by a baker transformation with a vertical stretching in the negative y direction. We have

$$\mathrm{T}(x,y)=\begin{cases}(y+k-\frac{1}{2},\,x-k+\frac{1}{2}) & k-\frac{1}{2}\leqslant x<k+\frac{1}{2},\quad 0\leqslant y<1\\ & k=0,1,2,\ldots,L\\ (y/2+k,\,2x-2k+1) & k-\frac{1}{2}\leqslant x<k,\quad 0\leqslant y<1\\ (y/2+k-\frac{1}{2},\,2x-2k) & k\leqslant x<k+\frac{1}{2},\quad 0\leqslant y<1\\ & k=\ldots,-2,-1;L+1,L+2,\ldots\end{cases}\tag{5.10}$$

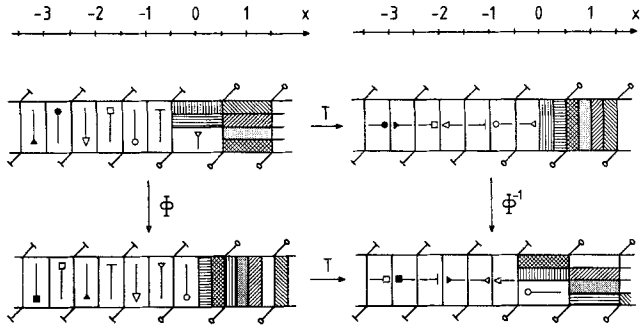

Fig. 23. Geometrical proof of the time-reversal symmetry of the open multibaker map at one end of the chain. The diagonals with circles are the axes of inversion of the corresponding squares under T. Diagonals with bars mean that T performs an inversion around this axis followed by a baker transformation with a stretching in the direction of the negative y axis.

T is defined on every point of $\mathcal{M}$. T is an involution ($T^2 = 1$). We note that time-reversal inside the chain fixes the form of the transformation T *outside* the chain.

5.2. Scattering Resonances

The treatment of the chain in the present scattering configuration is in all points identical to the treatment of Section 4.4.1 for the absorbing–absorbing boundary conditions. Accordingly, the decay rates are given by (4.18), but here with $m \geqslant 1$, since $m = 0$ is not compatible with the absorbing boundaries, as remarked in Section 4.2.1. The decay modes are obtained by solving the eigenvalue problem (2.19)–(2.20). Let

$$|\varphi\rangle = (u_0, v_0, u_1, v_1, ..., u_{L-1}, v_{L-1})^T \tag{5.11}$$

$$\langle\tilde{\varphi}| = (\tilde{u}_0, \tilde{v}_0, \tilde{u}_1, \tilde{v}_1, ..., \tilde{u}_{L-1}, \tilde{v}_{L-1}) \tag{5.12}$$

be the eigenvector and the adjoint eigenvector associated with the eigenvalue $\chi_m = 2 + 2\cos[m\pi/(L+1)]$ of A. We find the elements

$$u_k = v_{k-1} = c\{\sin(k\theta) + \sin[(k+1)\theta]\} \tag{5.13}$$

$$\tilde{u}_k = \tilde{v}_k = \tilde{c}\sin[(k+1)\theta] \tag{5.14}$$

with $k = 0, 1, 2, ..., L$ and the angle $\theta = (m\pi)/(L+1)$ $(1 \leqslant m \leqslant L)$. Some eigenvectors $|\varphi\rangle$ are drawn in Fig. 24.

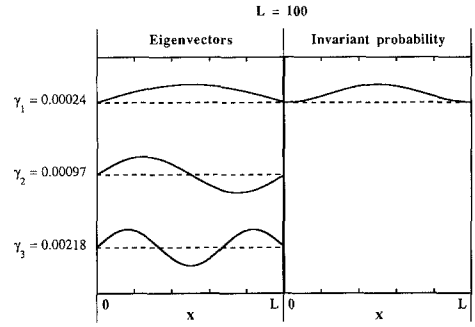

Fig. 24. Decay modes of the fractal repeller of the open and finite multibaker mapping of Fig. 21. The modes correspond to the complex scattering resonances of the family $\beta = 1$ and $m \geqslant 1$ ($L = 100$), together with the escape rates ($\tau = 1$). The left-hand column shows the eigenvectors $|\varphi\rangle$. The adjoint eigenvectors $\langle\tilde{\varphi}|$ of A have the same shape as $|\varphi\rangle$ on the scale of the figure. The right-hand column depicts the invariant probability $\{\pi_\alpha\}$ associated with the mode $m = 1$ of the fractal.

5.3. Invariant Probability Measure and Its Characteristic Quantities

Associated with the slowest decay rate is an invariant probability measure on the fractal repeller. By the Perron–Frobenius theorem, all the elements of the eigenvector (5.13) corresponding to χ_1 and of its adjoint (5.14) are positive since all the elements of A are positive or zero.

We can then construct a probabilistic Markov chain isomorph to the dynamics on the fractal repeller according to (2.31)–(2.33). The stationary probability is depicted in Fig. 24.

The characteristic quantities of chaos on the fractal repeller are given by (4.32)–(4.35) of Section 4.4.1, but with L replacing l. In particular, Fig. 25 shows how the exactly calculated escape rate behaves with the

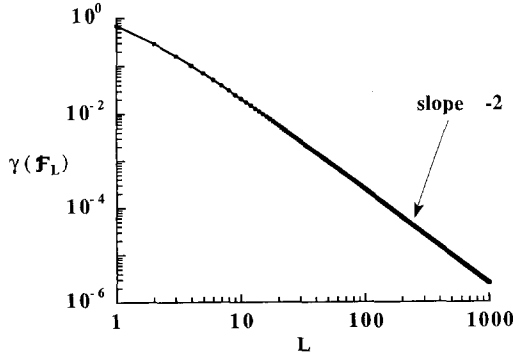

Fig. 25. Escape rate γ from the fractal repeller $\mathscr{F}_L$ versus the length L of the scatterer. The ordinate at the origin of the asymptote is related to the diffusion coefficient.

length L of the scatterer and we observe the approach to the diffusive behavior (4.33). The repeller is here also a simple fractal, with a trivial multifractal spectrum. For a large system, the fractal dimension tends to the value two, so that the fractal repeller fills the whole phase space in this limit.

5.4. Large-System Limit

The problem described here is an effusion out of the multibaker chain into free motion. At both ends of the chain, particles are leaking out with the escape rate (4.33). When the system is large ($L \to \infty$), the decay rates for $\beta = 1$ are given by (4.20) with the diffusion coefficient $\mathscr{D} = 1/4\tau$ (here $a = 1$) that was calculated in Section 3. As in Section 4.4.1, we observe that these decay rates, which are exactly derived from the Liouville dynamics of the system, approach the decay rates calculated from the diffusion equation (3.25) solved with absorbing boundaries at $x = 0$ and $x = L$. The solution of this problem is given by (4.22) but with the sum starting at $m = 1$. As previously, the phenomenological rates are approached by the exact decay rates when $L \to \infty$. Furthermore and in analogy with Section 4.2, we observe that the eigenvectors of the Liouville dynamics, namely (5.13), show the same shape as the corresponding eigenmodes of the phenomenological equation (see Fig. 24).

We conclude that decay and relaxation can be understood directly at the level of the Liouville dynamics without any recourse to stochastic assumption as done in standard kinetic theories. Although this result was obtained here in the case of a simple model, we believe that it can be generalized to more realistic systems like the Lorentz gas we described in ref. 9. The results of the present theory can be applied to other systems provided that their periodic orbits are all unstable of saddle type or that the stable periodic orbits can be shown to play a negligible role. In systems where forces may be attractive, stable periodic orbits may appear in physical processes involving the formation of molecular clusters which would remain thereafter undisturbed. At high temperature, the formation of bound particles is negligible, so that most periodic orbits would be of saddle type in such systems and the preceding results would apply to this dominant part of phase space which shows chaotic behaviors. In condensed phases like liquids or solids, we believe that similar considerations hold because of the numerical evidence reported in the introduction that the space-time entropy of these systems is positive. Since the KS entropy is a lower bound on the topological entropy per unit time, we may thus expect that the number of periodic orbits increases exponentially in such systems, a situation which is possible only for unstable periodic orbits. The generality

of the chaotic behaviors in nonlinear systems which was observed during the last decade leads us to expect that most periodic orbits are unstable in typical systems at room temperature which present irreversible processes and where the present theory is thus of application. We conjecture that, for a general nonequilibrium problem, the eigenvalues of the phenomenological equation will be given by the classical complex scattering resonances of the exact Liouville dynamics. These resonances naturally appear in the classical context in analogy with the equivalent concept in quantum scattering theory. In the limit of a large system, they approach the eigenvalues of the phenomenological equations, which are usually easier to derive than it is to solve the Liouville dynamics. Our purpose here was to show that there are no difficulties in principle to deriving transport properties in a straightforward way from the Liouville dynamics thanks to the scattering resonances. The concept of decay rate is thus defined at the level of the microscopic dynamics from the existence of trajectories of saddle type as they naturally arise in chaotic behaviors, in full agreement with the microscopic reversibility, which requires only that stretching along the unstable directions equals contraction along the stable directions. In this way, a bridge can be established between the microscopic reversible and the macroscopic irreversible dynamics.

Since the phenomenological equation is valid only in the limit of a large system and concerns only the slowest decay modes of the hydrodynamic dynamics, we may expect that growing discrepancies will appear between the exact resonances and the phenomenological ones related to the fast decay modes. Such a discrepancy already appears for large m's between the family $\beta = 1$ of exact resonances and the corresponding phenomenological ones. Furthermore, the exact Liouville dynamics presents new families of resonances which could not have been expected from the phenomenological equation, namely the scattering resonances (4.18)

$$\gamma_{m,\beta} \quad \text{for} \quad \beta \geqslant 2 \tag{5.15}$$

These decay rates are very large and concern the dynamics on times of the order of the inverse of the Lyapunov exponent directly related to the microscopic deterministic dynamics, which is ignored in the kinetic theories. The first of these fast decay rates appears at

$$\gamma_{1,2} = \frac{1}{\tau} \ln \frac{8}{1 + \cos[\pi/(L+1)]} \approx \frac{1}{\tau} \ln 4 + \mathscr{D} \left(\frac{\pi}{L}\right)^2 + \mathcal{O}(L^{-3}) \tag{5.16}$$

This rate is of the same order as decay rates in the slowest family, $\gamma_{m,1}$, when

$$m \approx 0.53L \tag{5.17}$$

which fixes a limit to the phenomenological equation. In (4.22), the use of the decay modes with m larger than (5.17) is therefore not justified. This limit corresponds to a time scale of the order of the inverse of the Lyapunov exponent

$$t \approx \frac{1}{\lambda} = \frac{\tau}{\ln 4} \tag{5.18}$$

On time scales shorter than the Lyapunov time, the dynamics follows the deterministic evolution. On longer time scales, the dynamics shows sensitivity to initial conditions and randomization at the basis of the macroscopic diffusion. Contrary to the standard kinetic theories, the origin

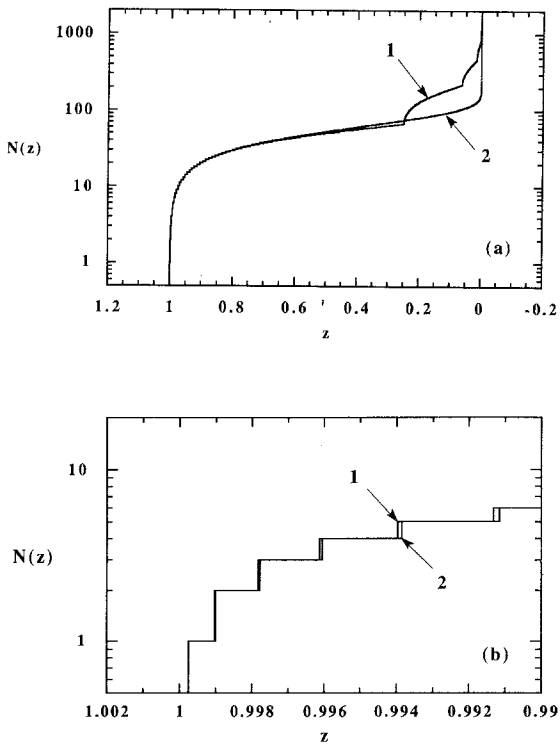

Fig. 26. (a) Comparison of the cumulative distribution functions $N(z)$ for the exact scattering resonances of the Liouville dynamics (1) and for the eigenvalues of the phenomenological diffusion equation (2) for a chain of length $L = 100$. We introduced $z = \exp(-\gamma)$ ($\tau = 1$). The bumps appearing near $z = 0$ on the distribution (1) of the exact resonances are due to the families $\beta = 2, 3, \ldots$ of scattering resonances; (b) enlargement of the distribution near the slowest resonances showing the slight discrepancy between the exact and the phenomenological dynamics in the hydrodynamic regime.

of randomization is now understood in terms of dynamical chaos and characterized quantitatively with the KS entropy per unit time and volume. The present theory reproduces the irreversible behaviors in the domain where it is expected and, furthermore, the theory is able to provide the limit of validity to the standard kinetic theories.

Figure 26 shows the cumulative distribution function for the decay rates of the Liouville dynamics compared with the eigenvalues of the diffusion equation. Defining $z = y^{-1}$, we introduced

$$N(z) \equiv \sum_{m=1}^{L} \sum_{\beta=1}^{\infty} \Theta(z - z_{m,\beta}) \tag{5.19}$$

where Θ is the Heaviside step function and

$$z_{m,\beta} = \frac{1}{4^{\beta}} \left(2 + 2 \cos \frac{m\pi}{L+1} \right), \qquad m = 1, 2, \ldots, L; \quad \beta = 1, 2, \ldots \tag{5.20}$$

and

$$z_m^{(\mathrm{ph})} = \exp - \left(\frac{m\pi}{2L} \right)^2, \qquad m = 1, 2, \ldots \tag{5.21}$$

The figures compare the cumulative distribution functions of the exact and approximate equations for a finite multibaker mapping with $L = 100$ cells. The phenomenological equation fairly reproduces the spectrum of the Liouville equation for the slow part of the dynamics given by the long-wavelength eigenmodes with $z \approx 1$. However, significant differences appear in the fast dynamics, which shows the limited validity of kinetic theories compared with a chaotic theory.

5.5. Diffusion and Chaotic Scattering

A deep relationship exists between large-scale diffusion and chaotic scattering which has been the object of recent studies.[8,37,38] Classical scattering has been described by an S-function which relates the ingoing trajectories to the outgoing ones in analogy with the quantum S-matrix. Work has shown that the outgoing trajectory may be an intricate function which is singular for the ingoing trajectories asymptotic to the fractal repeller. As a corollary, the time spent in the scatterer is also a singular function of the impact parameter. The open multibaker mapping also presents this phenomenon, as shown in Figs. 27 and 28, where we depict the exit time versus initial conditions along a vertical line at the end, $x = 0$, and in the middle, $x = 5$, of a chain of length $L = 10$. The fractal set of

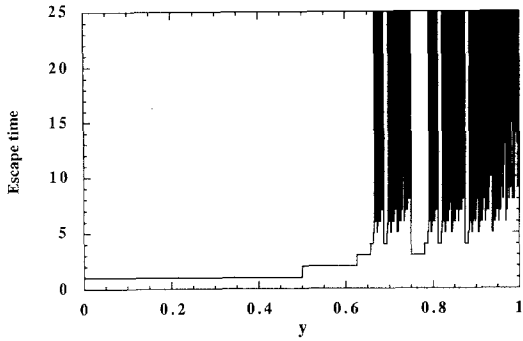

Fig. 27. Exit time function from the multibaker scatterer for initial conditions at $x = 0$ along the y axis for a chain of length $L = 10$. The exit time is the number of iterations to reach either $x < -1/2$ or $L + 1/2 \leqslant x$. The function appears to be singular on the fractal set of the intersections of $x = 0$ with the stable manifolds of the fractal repeller.

singularities of these functions has a fractal dimension given by half the fractal dimension of the repeller. In the large-system limit,

$$d_{\mathrm{I}} = d_{\mathrm{H}} = \frac{D_{\mathrm{H}}}{2} = 1 - \frac{1}{4 \ln 4}\left(\frac{\pi}{L}\right)^2 + \mathcal{O}(L^{-3}) \tag{5.22}$$

[cf. (4.35)]. We observe that the singularities fill the whole set of incoming trajectories for a large system.

In scattering processes, the fractal repeller is formed by trajectories which are trapped in the scatterer. A nonequilibrium constraint is not required to select the fractal repeller, which is intrinsic to the scattering process. In this context, we recently showed for the Lorentz gas that the

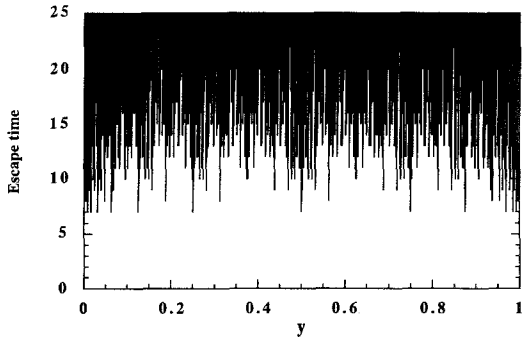

Fig. 28. Same as Fig. 27, but at the middle $x = 5$ of the chain of length $L = 10$. The function is symmetrical for an inversion with respect to $y = 0.5$ up to numerical errors.

diffusion coefficient appears in the quantities characterizing the chaotic scattering.[9] For the open multibaker chain, the formula (4.36) relating chaotic scattering to diffusion is also of application and is derived in the same way as in Section 4.4.1 for the fractal repeller $\mathscr{F}_L$ in the system of length L. In the limit $L \to \infty$, the KS entropy equals the Lyapunov exponent and we recover the Pesin formula.[15] This result seems to have a large application range. It concerns not only systems with a two-dimensional Poincaré section such as the multibaker chain or the 2D Lorentz gas, but also many-body systems such as hard-sphere gases and their transport properties, as discussed in the conclusions.

6. CONCENTRATION GRADIENT IN THE OPEN AND FINITE MULTIBAKER CHAIN

6.1. Fick's Law

We consider that a concentration gradient is applied to the open multibaker chain defined in Section 5. A continuous flow of particles is scattered by the multibaker chain. The concentration of particles arriving from the left is ρ_- and the concentration of particles arriving from the right is ρ_+, which is in general different from ρ_-. The chain is thus permanently occupied with a distribution of particles that we want to determine. The dynamics occurs on the set of trajectories which are not trapped by the scatterer. This set is complementary to the set composed of the fractal repeller and its invariant manifolds. The invariant probability measure is defined by requiring that at each time step, the incoming cells of the partition $\omega = -1$ at the left side and $\omega = 2L$ at the right side are uniformly covered according to Poisson distributions. The number of particles in the cell $\omega = -1$ (resp. $\omega = 2L$) of area $1/2$ is a random variable N_- (resp. N_+) such that

$$\text{Prob}\{N_\pm = n\} = \frac{1}{n!} e^{-\rho_\pm/2} \left(\frac{\rho_\pm}{2}\right)^n \tag{6.1}$$

The distributions (6.1) also hold for each ingoing cells arriving from minus and plus infinity, respectively. The stochastic process sodefined is called a Poisson suspension over the dynamical system.[42] The scatterer acts on the incoming distributions by stretching and cutting according to its own dynamics so that the outgoing cells are covered with a pattern formed by vertical strips with a density ρ_+ and ρ_- whether the strip is issued from plus or minus infinity. Because of the fractal repeller, finer and finer strips accumulate along the unstable manifolds of the fractal repeller. The strips

are composed of trajectories of type I in the notation of (5.7)–(5.8), so that there is a countable set of strips which are labeled by the strings

$$\omega_1 \omega_2 \cdots \omega_{n+1} \tag{6.2}$$

with

$$\begin{aligned} \omega_1 &\in \{-1, 2L\} \\ \omega_m &\in \{0, 1, 2, \ldots, 2L-1\}, \qquad (m = 2, \ldots, n) \\ \omega_{n+1} &\in \{-2, 2L+1\} \end{aligned} \tag{6.3}$$

ω_1 is necessarily the symbol of one of the two ingoing cells, either -1 or $2L$, while ω_{n+1} is the symbol of one of the two outgoing cells, either -2 or $2L+1$. In this section, we included four extra cells of the partition of Section 5 in the alphabet (see Figs. 21 and 29).

The distributions (6.1) induce in the system a nonequilibrium ensemble defined with a measure which is absolutely continuous with respect to the Lebesgue measure. The phase space is divided into a countable set of rectangles where the density is either ρ_+ or ρ_-. If we average the nonequilibrium measure in each cell of the generating partition, we find densities $\{\rho_\alpha\}$ having values between ρ_+ and ρ_- that we want to calculate. According to the geometry of the system shown in Figs. 21 and 29, these densities are given as solutions of the equation

$$\sum_{\alpha=-2}^{2L+1} \rho_\alpha R_{\alpha\beta} = \rho_\beta \tag{6.4}$$

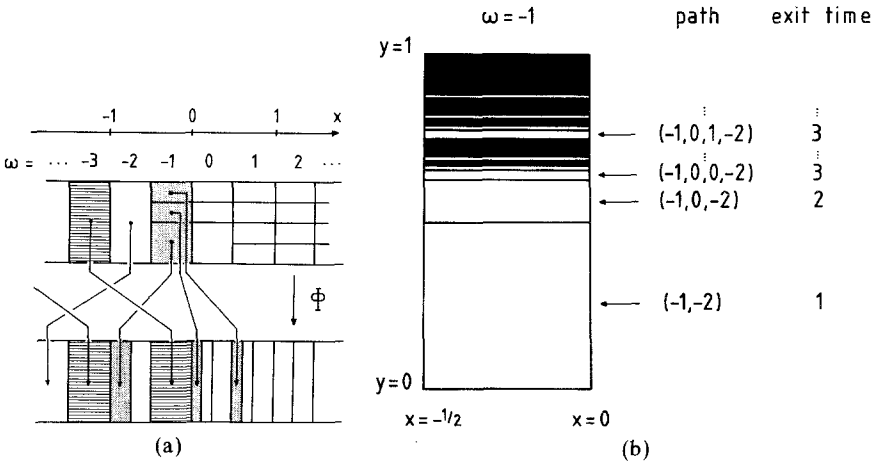

Fig. 29. (a) Open multibaker mapping Φ acting on ingoing particles at the left-hand end of the chain; (b) partition of the ingoing cell $\omega = -1$ by the stable manifolds of the fractal repeller with the strings $\omega_1 \cdots \omega_{n+1}$ labeling the horizontal strips of the partition together with the corresponding exit times.

where R is the matrix

$$R = \begin{cases} 1/2 & \alpha = -1, 0; \quad \beta = -2 \\ & \alpha = 2L-1, 2L; \quad \beta = 2L+1 \\ 1/4 & \alpha = -1, 0; \quad \beta = 0, 1 \\ & \alpha = 2k-1, 2k; \quad \beta = 2k-2, 2k-1, 2k, 2k+1 \\ & (k = 1, \ldots, L-1) \\ & \alpha = 2L-1, 2L; \quad \beta = 2L-2, 2L-1 \\ 0 & \text{otherwise} \end{cases} \tag{6.5}$$

For $L = 4$, R has the form

$$R = \begin{array}{c} \\ -2 \\ -1 \\ 0 \\ 1 \\ 2 \\ 3 \\ 4 \\ 5 \\ 6 \\ 7 \\ 8 \\ 9 \end{array} \begin{array}{c} \begin{array}{cccccccccccc} -2 & -1 & 0 & 1 & 2 & 3 & 4 & 5 & 6 & 7 & 8 & 9 \end{array} \\ \left[\begin{array}{cccccccccccc} & & & & & & & & & & & \\ 1/2 & & 1/4 & 1/4 & & & & & & & & \\ 1/2 & & 1/4 & 1/4 & & & & & & & & \\ & & 1/4 & 1/4 & 1/4 & 1/4 & & & & & & \\ & & 1/4 & 1/4 & 1/4 & 1/4 & & & & & & \\ & & & & 1/4 & 1/4 & 1/4 & 1/4 & & & & \\ & & & & 1/4 & 1/4 & 1/4 & 1/4 & & & & \\ & & & & & & 1/4 & 1/4 & 1/4 & 1/4 & & \\ & & & & & & 1/4 & 1/4 & 1/4 & 1/4 & & \\ & & & & & & & & 1/4 & 1/4 & & 1/2 \\ & & & & & & & & 1/4 & 1/4 & & 1/2 \\ & & & & & & & & & & & \end{array}\right] \end{array} \tag{6.6}$$

The solution of (6.4) is

$$\rho_{2k} = \rho_{2k+1} = \frac{\rho_+ - \rho_-}{L+1}(k+1) + \rho_- \tag{6.7}$$

$$\cdots = \rho_{-2} = \rho_- + \frac{1}{2}\frac{\rho_+ - \rho_-}{L+1}$$

$$\rho_+ - \frac{1}{2}\frac{\rho_+ - \rho_-}{L+1} = \rho_{2L+1} = \cdots \tag{6.8}$$

When $\rho_+ = \rho_- = \rho$, the whole system is covered by the equilibrium uniform distribution as expected. In the case $\rho_+ \geqslant \rho_-$ drawn in Fig. 30, we

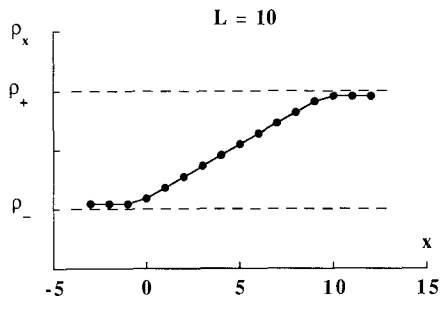

Fig. 30. Fickian density profile $\{\rho_x\}$ across the chain under a nonequilibrium concentration gradient $\rho_+ > \rho_-$.

observe that the solution has the usual linear dependence with the gradient of concentration. Accordingly, Fick's law is satisfied for the multibaker chain. We note that the outgoing densities at the left and right sides are nearly equal to the corresponding incoming densities ρ_+ and ρ_- but they are moderated by a small quantity of order $1/(L+1)$.

An important remark is the following. Fick's law is established in the system when the distributions in the ingoing cells $\omega = -1$ and $\omega = 2L$ are uniform. It is always possible to choose adequately the distributions so that the concentration gradient does not obey Fick's law. However, these non-Fickian densities are exceptional for the following reason. These special distributions must be determined according to the precise forms and locations of the stable manifolds of the fractal repeller. Indeed, the stable manifolds divide the ingoing cells $\omega = -1$ and $\omega = 2L$ into horizontal strips (Fig. 29). The densities in each of the horizontal strips should be suitably chosen in order to produce an exceptional density profile. However, for that purpose, we need to know the stable manifolds and to send the incoming particles with complete control for the impact parameter to fall in the right horizontal strip. Because external systems have their own dynamics which does not carry out in general such processes, it is the Fick law that is observed in the real world.

In previous sections, the KS entropy per unit time was defined for an invariant measure over a set of bounded trajectories. Since the stochastic processes considered in previous sections are isomorph to discrete Markov chains, their KS entropy was finite and positive. However, for scattering processes with a continuous flow of particles, such as the Poisson suspension defined by (6.1), the KS entropy per unit time is no longer finite and must be generalized into an ε-entropy per unit time to characterize dynamical randomness.[55,56] At equilibrium and in the limit of a long chain, the

ε-entropy per unit time can be shown to increase linearly with the length of the chain so that we recover the space-time entropy (3.26). These results are reported elsewhere.[66]

7. CONCLUSIONS

In the present paper, several new and different concepts have been introduced to study nonequilibrium problems. We illustrated these concepts with a simple dynamical model, the multibaker chain, which is exactly solvable. The multibaker chain is of large spatial extension and presents dynamical chaos in relation to transport in the form of diffusion, so that it mimics the dynamics of systems which are studied in nonequilibrium statistical mechanics. It allows us to bridge the gap between microscopic and macroscopic dynamics. The multibaker chain can be put in a closed, finite or infinite container or be adapted for a gedanken scattering experiment. We showed that the time evolution of the closed multibaker chain is described by a unitary operator which has a continuous spectrum characterized by the complex resonances, all of which can be calculated exactly. The slowest of the complex resonances reproduce nicely the eigenvalues of the diffusion equation solved for the corresponding boundary conditions. There is thus a quasi spectral isomorphism between the dynamics of the exact Liouville equation and that of the phenomenological irreversible equation of diffusion. This result is one of the strongest possible justifications for the use of the irreversible equations.

Nonequilibrium states can then be constructed by different kinds of nonequilibrium conditions defined by absorbing boundaries or fixed frequencies of residence in certain regions of phase space. The sets of trajectories which satisfy these nonequilibrium conditions are highly unstable and of zero Lebesgue measure. Nevertheless, these nonequilibrium sets are not empty, but are Cantor sets forming a fractal repeller. The rate of escape, which is the slowest resonance for the dynamics on the fractal repeller, gives the lifetime of the nonequilibrium state. When the nonequilibrium conditions are of hydrodynamic nature, the escape rates are small and appear to be identical to the decay rate given by the diffusion equation.

We analyzed several nonequilibrium conditions to show the variety of fractal repellers that can be obtained for one-particle or many-particle systems. A fractal repeller is thus associated with each nonequilibrium state. When the nonequilibrium constraint is relaxed, we obtain the equilibrium state and the fractal repeller occupies the whole phase space. In chaotic dynamical systems where all the trajectories are of saddle type with positive Lyapunov exponents, each nonequilibrium state is thus unstable

with respect to the equilibrium state as required by the second law of thermodynamics. This result, which seems general, is expressed by a formula which gives the diffusion coefficient in terms of the difference between the Lyapunov exponent and the KS entropy of the nonequilibrium fractal repeller (4.36).[9] The magnitude of the Lyapunov exponent and the KS entropy are in general different from the magnitude of the diffusion escape rate since they are quantities playing a role at different levels of the dynamics. The Lyapunov exponents and the KS entropy concern the short-time dynamics, while the diffusion escape rate concerns the long-time dynamics of large spatial extension. In nonequilibrium conditions, both dynamics are related to each other through chaotic scattering,[35] and the formula (4.36) results.[9]

As we already emphasized in the Introduction, dynamical chaos is a phenomenon in itself occurring in the microscopic dynamics of large and many-body systems offering us a unique opportunity to understand the origin of stochasticity in these deterministic systems without the controversial assumptions of kinetic theories. We now see better that the KS entropy per unit time of the microscopic dynamics provides us with a quantitative measure of dynamical randomness.

In Section 5 we showed how chaotic scattering is related to the statistical aspects of diffusion. In scattering processes on large systems, the scattering functions are very irregular due to the fractal repeller of trapped trajectories and this irregularity is related to the transport processes.

In Section 6 the scattering process was turned into a typical nonequilibrium process with a concentration gradient across the scatterer. Fick's law was shown to be valid here also because of the dynamical instability which prevents the occurrence of non-Fickian profiles.

Although the concepts introduced in the present paper were applied to the multibaker chain, we believe that they are general and can be applied to more realistic systems. The multibaker chain shares several properties with the periodic[21,22] or random[67] Lorentz gases in which most of the previous concepts can also be studied. Besides such models with a few degrees of freedom, hard-sphere or hard-disk fluids can also be treated by these methods. The nonequilibrium fractal repellers of Sections 4 and 5 can be considered in hard-sphere or Lennard-Jones gases in nonequilibrium conditions.[68,69] For instance, if the gas container is punctured by a small hole, there is effusion of the gas out of the container. In the spirit of Section 4.8, a fractal repeller is defined as the set of trajectories where the particles are trapped in the container, a situation which is highly unstable. The escape rate of this repeller is related to the effusion rate of the gas. In the experiment where two containers are connected to each other through a small hole, there are fluctuations in the number of particles in each reser-

voir although the total number of particles in both reservoirs is constant. The lifetime of the fluctuations can be studied by extending the method of Sections 4.6 and 4.8. Heat conduction or viscosity can be treated in a similar way by considering the fractal repeller formed by the highly unstable set of trajectories where the total energy or momentum in a region of the system remains higher than the equilibrium ones. The decay rate from such a nonequilibrium condition could be calculated with Navier–Stokes equations in order to see how the rate depends on the transport coefficients and the geometry of absorbing boundary. On the other hand, we can conjecture that the escape rate from a so-defined fractal repeller is given as the difference between the sum of Lyapunov exponents and the KS entropy. Accordingly, the transport coefficients would be given in terms of the quantities characterizing the dynamical chaos of the fractal repeller.

Of great theoretical interest are the fractal repellers obtained in trajectory reconstruction when a measuring device observes a gas of hard spheres, for instance. The results of Section 4.7 suggest that the information dimension of fractal sets reconstructed from a given trajectory is close to the phase space dimension when the partition built by the observing device is rough, while this information dimension decreases to zero when the

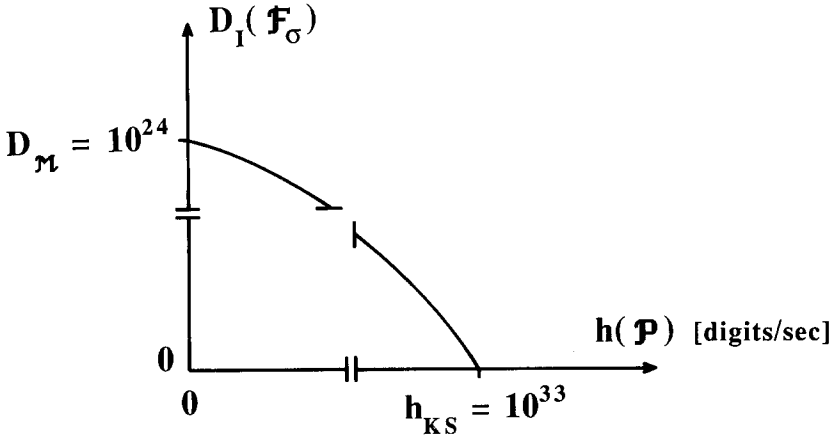

Fig. 31. Schematic diagram of the information dimension of the fractal set obtained by trajectory reconstruction from the data produced by a measuring device observing a mole of gas with a resolution characterized by the entropy per unit time $h(\mathcal{P})$ of the partition $\mathcal{P}$ of phase space into the resolution cells. For a low-resolution derive, the phase space is resolved into fractal sets of dimension close to the phase space dimension of the mole of particles, namely $D_{\mathcal{M}} \sim 6N_{Av} \sim 10^{24}$. On the other hand, for a hypothetical high-resolution device, the entropy of which is close to the KS entropy of the gas ($\sim 10^{33}$ digits/sec mole), the dimension of the fractal set drops to zero in the limit of perfect resolution into distinct trajectories.

partition becomes finer and finer and its entropy reaches the KS entropy of the system. For such partitions like the generating partition, the observation of the dynamics can be resolved into individual trajectories. Otherwise, the measuring device can only distinguish fractal sets whose information dimension is not much smaller than the phase space dimension. This behavior is schematically represented in Fig. 31. Because the accumulation rate of data of the available measuring devices is very small compared to the KS entropy of the gas calculated in the introduction, we cannot expect trajectory resolution for typical gases and we understand in this way the success of the Boltzmann equation based on smooth one-particle densities.

The properties described in the present paper are deeply related to the fact that the entropy per unit time and volume is positive for many-body interacting classical systems. We remark here that a definition of dynamical entropy is also available for many-body quantum systems as shown by Connes *et al.*[70] Accordingly, we believe that some of the previous considerations can be extended to the quantum description.

APPENDIX

In this Appendix, we construct some fractal repeller related to the dyadic expansion of real numbers given by the following map of the unit interval:

$$\Phi(x) = 2x \pmod 1 \tag{A.1}$$

Our purpose is to show that, for this simple map, some of the fractals considered in Section 4 reduce to known examples.

A.1. The Eggleston–Billingsley Problem

We define the set of real numbers for which the dyadic expansion contains 1 with the frequency $0 \leqslant \alpha < 1$,

$$Y(\alpha) = \left\{ x \in [0.1[: \frac{1}{n} \sum_{m=0}^{n-1} I_1(\Phi^m x) \xrightarrow[n \to \infty]{} \alpha \right\} \tag{A.2}$$

where

$$I_1(x) = \begin{cases} 1 & \text{for } 1/2 \leqslant x < 1 \\ 0 & \text{otherwise} \end{cases} \tag{A.3}$$

The dynamical system (A.1) is known to be isomorph to a Bernoulli process on the symbols $\{0, 1\}$ with probabilities $(1/2, 1/2)$, so that the Markov chain matrix and its invariant probability are

$$P = \begin{pmatrix} 1/2 & 1/2 \\ 1/2 & 1/2 \end{pmatrix}, \qquad \text{with} \quad p = (1/2 \quad 1/2) \tag{A.4}$$

and the matrix (4.64) is here

$$R = \begin{array}{c} \\ 0 \\ 1 \end{array} \begin{array}{c} \begin{array}{cc} 0 & 1 \end{array} \\ \begin{pmatrix} 1/2 & e^{\beta}/2 \\ 1/2 & e^{\beta}/2 \end{pmatrix} \end{array} \tag{A.5}$$

with the eigenvalues 0 and $(e^{\beta}+1)/2$. The generating function (4.66) is thus

$$G(\beta) = \ln \frac{1+e^{\beta}}{2} \tag{A.6}$$

and its Legendre transform (4.54)–(4.55) is

$$F(\alpha) = -\alpha \ln \alpha - (1-\alpha)\ln(1-\alpha) - \ln 2 \tag{A.7}$$

which gives minus the escape rate. These functions are drawn in Fig. 32. According to (4.58), with ln 4 replaced by the Lyapunov exponent ln 2 of the map (A.1), the Hausdorff dimension of the set $Y(\alpha)$ is then

$$d_H = \frac{1}{\ln 2}\left[-\alpha \ln \alpha - (1-\alpha)\ln(1-\alpha)\right] \tag{A.8}$$

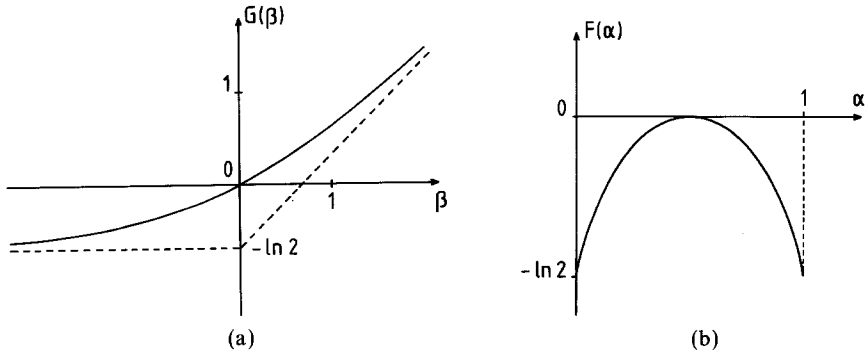

Fig. 32. (a) Generating function $G(\beta)$ of the residence time in the interval $1/2 \leqslant x < 1$ for the map $x \to 2x$ (mod 1) of the unit interval; (b) Legendre transform $F(\alpha)$ of $G(\beta)$ giving the escape rate out of the fractal set of trajectories spending a fraction α of time in the interval $1/2 \leqslant x < 1$.

which is the formula given by Eggleston[71] and Billingsley.[12] The KS entropy of $Y(\alpha)$ is then

$$h_{KS} = -\alpha \ln \alpha - (1-\alpha)\ln(1-\alpha) \tag{A.9}$$

A.2. Many Independent Particles in the Unit Interval

The trajectories for one particle moving under the mapping (A.1) in the unit interval $\mathcal{I}$ are in one-to-one correspondence with infinite sequence of 0 and 1

$$\underline{\omega} = \omega_0 \omega_1 \omega_2 \cdots \tag{A.10}$$

We assume here that N independent particles move on the unit interval under (A.1). The phase space is now $\mathcal{I} \otimes \mathcal{I} \otimes \cdots \otimes \mathcal{I}$ and the trajectories of the system are described by simply infinite sequences composed at each iteration of N-tuples of the symbols 0 and 1 [cf. (4.88)]. At each instant of time, 2^N different states are possible, so that the KS entropy per unit time is

$$\lambda = h_{KS} = N \ln 2 \tag{A.11}$$

corresponding to the invariant measure (4.90) with $p_\omega = 1/2$. A nonequilibrium condition can be imposed on the system selecting trajectories $\underline{\Omega}$ such that a certain number of particles is always present in the right-hand half of the unit interval,

$$M_1 \leqslant \sum_{i=1}^{N} \omega_n^{(i)} \leqslant M_2, \qquad \text{with} \quad 1 \leqslant M_1 \leqslant M_2 \leqslant N \tag{A.12}$$

The examples of an invariant set for $N=2$ are depicted in Fig. 33. Imposing the condition where $M_1 = 1$ but $M_2 = 2$ select a fractal repeller in phase space which is a Sierpinski gasket[72] with a KS entropy of

$$h_{KS} = \ln 3 < \lambda = \ln 4 \tag{A.13}$$

and a Hausdorff dimension

$$D_H = \frac{\ln 3}{\ln 2} \tag{A.14}$$

This example illustrates the formation of a fractal repeller in a dynamics with several independent particles by a nonequilibrium condition on the number of particles in some domain of phase space.

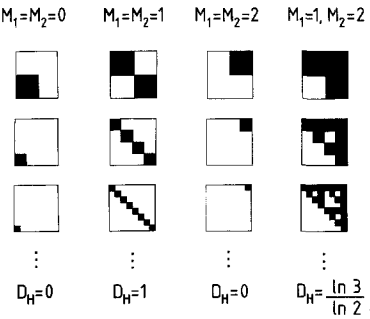

Fig. 33. Examples of fractal and nonfractal repellers generated in the system of two independent particles moving under the mapping $x \to 2x \pmod 1$ in the unit interval. The first column depicts the generation of the invariant set under the condition that both particles are always in $0 \leqslant x < 1/2$. The single trajectory $x_1 = x_2 = 0$ is selected and $D_H = 0$. The second column corresponds to the condition that a particle is always in $0 \leqslant x < 1/2$ and the other in $1/2 \leqslant x < 1$. A line of initial conditions is selected and $D_H = 1$. The third column corresponds to a similar condition as in the first one except that here both particles must be in $1/2 \leqslant x < 1$. The trajectory $x_1 = x_2 = 1$ is now selected and $D_H = 0$. The fourth column shows the generation of a Sierpinski gasket under the condition that the interval $1/2 \leqslant x < 1$ is occupied at each iteration by at least one particle. In this case, $D_H = \ln 3/\ln 2$.

When the number N of particles is large so that

$$\frac{M_1}{N} = \frac{M_2}{N} = f \tag{A.15}$$

then the KS entropy becomes

$$h_{KS} = N[-f \ln f - (1-f)\ln(1-f)] \tag{A.16}$$

and the Hausdorff dimension

$$D_H = \frac{N}{\ln 2}[-f \ln f - (1-f)\ln(1-f)] \tag{A.17}$$

We observe a similarity with the results of Section A.1. If we require that the N independent particles spend a fraction $f = \alpha$ of their time in the domain 1, then the same KS entropy and Hausdorff dimension per particle would be obtained as with the instantaneous condition of the present section.

ACKNOWLEDGMENTS

It is a pleasure to thank Prof. G. Nicolis for support, encouragement, and his numerous contributions to this work during discussions. I received

important suggestions from D. Ruelle and J.-P. Eckmann. This work owes much to Prof. I. Prigogine, as well as to Profs. S. A. Rice and R. Kapral. I am grateful to H. Hasegawa for his suggestions regarding the text. I also thank I. Antoniou, P. Cvitanović, Y. Elskens, T. Hudetz, M. Mareschal, D. Rand, T. Tél, W. Thirring, and X.-J. Wang for fruitful discussions. This work is financially supported by the National Fund for Scientific Research (Belgium) under the program "Chercheur Qualifié."

REFERENCES

1. N. N. Krylov, ed., *Works on the Foundations of Statistical Mechanics* (Princeton University Press, 1979); Ya. Sinai, in *Works on the Foundations of Statistical Mechanics*, N. N. Krylov, ed. (Princeton University Press, 1979), pp. 239–281.
2. Ya. G. Sinai, On the entropy per particle for the dynamical system of hard spheres, preprint (1978).
3. Ya. G. Sinai and N. I. Chernov, *Russian Math. Surveys* **42**(3):181–207 (1987).
4. H. A. Posch and W. G. Hoover, *Phys. Rev. A* **38**:473–482 (1988); **39**:2175–2188 (1989).
5. D. J. Evans, E. G. D. Cohen, and G. P. Morris, *Phys. Rev. A* **42**:5990–5997 (1990).
6. P. Gaspard and G. Nicolis, *Physicalia Mag. (J. Belg. Phys. Soc.)* **7**:151–191 (1985).
7. P. Gaspard, What is the role of dynamical chaos in irreversible processes? in *Solitons and Chaos*, I. Antoniou and F. Lambert, eds. (Springer, Berlin, 1991), pp. 46–57.
8. P. Gaspard and S. A. Rice, *J. Chem. Phys.* **90**:2225–2241 (1989); **91**:3279 (1989).
9. P. Gaspard and G. Nicolis, *Phys. Rev. Lett.* **65**:1693–1696 (1990).
10. A. J. Lieberman and A. J. Lichtenberg, *Regular and Stochastic Motion* (Springer, New York, 1983).
11. V. I. Arnold and A. Avez, *Ergodic Problems of Classical Mechanics* (Benjamin, New York, 1968).
12. P. Billingsley, *Ergodic Theory and Information* (Wiley, New York, 1965).
13. Ya. G. Sinai, ed., *Dynamical Systems II* (Springer, Berlin, 1989).
14. J.-P. Eckmann and D. Ruelle, *Rev. Mod. Phys.* **57**:617 (1985).
15. Ya. B. Pesin, *Math. USSR Izv.* **10**(6):1261 (1976); *Russ. Math. Surveys* **32**(4):55 (1977).
16. S. Goldstein, J. L. Lebowitz, and M. Aizenmann, in *Dynamical Systems, Theory and Applications*, J. Moser, ed. (Springer, Berlin, 1975), p. 112.
17. A. Brandstäter, J. Swift, H. L. Swinney, A. Wolf, J. D. Farmer, E. Jen, and J. P. Crutchfield, *Phys. Rev. Lett.* **51**:1442 (1983).
18. J. Wisdom, S. J. Peale, and F. Mignard, *Icarus* **58**:137–152 (1984).
19. P. Gaspard, Bound, quasi-bound, and resonant quantum states: Dynamical and statistical aspects, in *Quantum Chaos*, H. A. Cerdeira, R. Ramaswamy, M. C. Gutzwiller, and G. Casati, eds. (World Scientific, Singapore, 1991, p. 348).
20. R. S. MacKay, J. D. Meiss, and I. C. Percival, *Physica D* **13**:55–81 (1984); D. Bensimon and L. P. Kadanoff, *Physica D* **13**:82–89 (1984).
21. E. Hopf, *Ergodentheorie* (Chelsea, New York, 1948).
22. C. Grebogi, E. Ott, and J. A. Yorke, *Phys. Rev. A* **37**:1711–1724 (1988).
23. S. Smale, *The Mathematics of Time* (Springer, New York, 1980).
24. Y. Elskens and R. Kapral, *J. Stat. Phys.* **38**:1027–1049 (1985).
25. L. A. Bunimovich and Ya. G. Sinai, *Commun. Math. Phys.* **78**:247, 479 (1980).
26. J. Machta and R. Zwanzig, *Phys. Rev. Lett.* **50**:1959 (1983); *J. Stat. Phys.* **32**:555 (1983).

27. R. Bowen, *Equilibrium States and the Ergodic Theory of Anosov Diffeomorphisms* (Springer, Berlin, 1975).
28. D. Ruelle, *Thermodynamic Formalism* (Addison-Wesley, Reading, Massachusetts, 1978); D. Ruelle, *Commun. Math. Phys.* **125**:239–262 (1989).
29. D. Mayer, *Commun. Math. Phys.* **95**:1–15 (1984); D. Mayer and G. Roepstorff, *J. Stat. Phys.* **47**:149–171 (1987); **50**:331–344 (1988).
30. R. Artuso, E. Aurell, and P. Cvitanović, *Nonlinearity* **3**:325–359, 361–386 (1990); P. Cvitanović and B. Eckhardt, *J. Phys. A: Math. Gen.* **24**:L237 (1991); B. Eckhardt, *J. Phys. A: Math. Gen.* **20**:5971–5979 (1987).
31. D. Ruelle, *Phys. Rev. Lett.* **56**:405–407 (1986); *J. Stat. Phys.* **44**:281–292 (1986); *C. R. Acad. Sci. Paris I* **296**:191–193 (1983).
32. J.-P. Eckmann, Resonances in dynamical systems, in *Proceedings of the IXth International Congress on Mathematical Physics* (IOP Publishing, 1989), pp. 192–207; V. Baladi, J.-P. Eckmann and D. Ruelle, *Nonlinearity* **2**:119–135 (1989).
33. S. Isola, *Commun. Math. Phys.* **116**:343–352 (1988).
34. F. Christiansen, G. Paladin, and H. H. Rugh, *Phys. Rev. Lett.* **65**:2087–2090 (1990).
35. B. O. Koopman, *Proc. Natl. Acad. Sci. USA* **17**:315 (1931).
36. I. Prigogine, *Non-Equilibrium Statistical Mechanics* (Wiley, New York, 1962).
37. D. W. Noid, S. K. Gray, and S. A. Rice, *J. Chem. Phys.* **84**:2649 (1986); C. Jung and H. J. Scholz, *J. Phys. A: Math. Gen.* **20**:3607 (1987); M. Hénon, *Physica D* **33**:132 (1988); G. Troll and U. Smilansky, *Physica D* **35**:34 (1989); S. Bleher, E. Ott, and C. Grebogi, *Physica D* **46**:87–121 (1990); Z. Kovács and Tamás Tél, *Phys. Rev. Lett.* **64**:1617 (1990); P. Eckelt and E. Zienicke, *J. Phys. A: Math. Gen.* **24**:153–173 (1991); R. A. Jalabert, H. U. Baranger, and A. D. Stone, *Phys. Rev. Lett.* **65**:2442–2445 (1990).
38. T. Tél, Transient chaos, preprint (1990).
39. P. Walters, *An Introduction to Ergodic Theory* (Springer, Berlin, 1981).
40. J. Moser, *Stable and Random Motions in Dynamical Systems* (Princeton University Press, 1973).
41. L. P. Kadanoff and C. Tang, *Proc. Natl. Acad. Sci. USA* **81**:1276 (1984); P. Szépfalusy and T. Tél, *Phys. Rev. A* **34**:2520 (1986).
42. I. P. Cornfeld, S. V. Fomin, and Ya. G. Sinai, *Ergodic Theory* (Springer, New York, 1982).
43. S. A. Rice, P. Gaspard, and K. Nakamura, *Adv. Class. Traj. Meth.* **1**:215–313 (1992).
44. F. R. Gantmacher, *Applications of the Theory of Matrices* (Interscience, New York, 1959).
45. D. Ornstein, *Science* **243**:182 (1989).
46. H. Kantz and P. Grassberger, *Physica D* **17**:75 (1985); T. Bohr and D. Rand, *Physica D* **25**:387 (1987).
47. T. C. Halsey, M. H. Jensen, L. P. Kadanoff, I. Procaccia, and B. I. Shraiman, *Phys. Rev. A* **33**:1141 (1986).
48. D. Ruelle, in *Scaling and Self-Similarity in Physics*, J. Fröhlich, ed. (Birkhäuser, Boston, 1983), pp. 351–357.
49. L.-S. Young, *Ergod. Theory Dynam. Syst.* **2**:109 (1982).
50. D. A. McQuarrie, *Statistical Mechanics* (Harper & Row, New York, 1976).
51. M. E. Ratner, *Sov. Math. Dokl.* **10**(3):629–631 (1969).
52. J. L. Doob, *Stochastic Processes* (Wiley, New York, 1953).
53. I. A. Ibragimov, *Theory Prob. Appl.* **7**:349–382 (1962).
54. H. Spohn, *Rev. Mod. Phys.* **53**:569 (1980).
55. A. N. Kolmogorov, *IRE Trans. Inform. Theory* **1**:102 (1956); V. M. Tikhomirov, *Russ. Math. Surveys* **18**:51 (1963).
56. P. Gaspard and X.-J. Wang, in preparation.
57. T. Geisel, J. Nierwetberg, and A. Zacherl, *Phys. Rev. Lett.* **54**:616–619 (1985).

58. S. Grossmann and H. Fujisaka, *Phys. Rev. A* **26**:1779–1782 (1982).
59. S. Thomae, Chaos-induced diffusion, in *Statics and Dynamics of Nonlinear Systems*, G. Benedek *et al.*, eds. (Springer, Berlin, 1983), pp. 204–210.
60. M. Schell, S. Fraser, and R. Kapral, *Phys. Rev. A* **26**:504–521 (1982).
61. G. H. Weiss, *J. Stat. Phys.* **42**:3 (1986).
62. R. S. Ellis, *Entropy, Large Deviations, and Statistical Mechanics* (Springer, New York, 1985).
63. M. C. Mackey, *Rev. Mod. Phys.* **61**:981–1015 (1989).
64. I. Prigogine, *From Being to Becoming: Time and Complexity in the Physical Sciences* (Freeman, San Francisco, 1980).
65. G. Nicolis and C. Nicolis, *Phys. Rev. A* **38**:427 (1988).
66. P. Gaspard, Entropy per unit time for scattering processes, in preparation.
67. H. Van Beijeren, *Rev. Mod. Phys.* **54**:195 (1982).
68. M. Mareschal and E. Kestemont, *Nature* **323**:427 (1987).
69. M. Mareschal, M. Malek-Mansour, A. Puhl, and E. Kestemont, *Phys. Rev. Lett.* **61**:2550 (1988).
70. A. Connes, H. Narnhofer, and W. Thirring, *Commun. Math. Phys.* **112**:691 (1987).
71. H. G. Eggleston, *Q. J. Math. Oxford Ser.* **20**:31–36 (1949).
72. B. Mandelbrot, *The Fractal Geometry of Nature* (Freeman, San Francisco, 1982).